Atmospheric Research 336 (2026) 108829

Contents lists available at ScienceDirect

Atmospheric Research

journal homepage: www.elsevier.com/locate/atmosres

Dipole patterns of spring precipitation in northeast China: Links to Kara Sea Ice and Eurasian snow cover

Xinya Shu [a], Shanshan Wang [a,b,*], Yuanyuan Hu [a], Yiwei Pang [a], Hao Wang [a], Yongli He [a], Fei Ji [a], Jianping Huang [a,b], Jinxia Zhang [a]

[a] Key Laboratory for Semi-Arid Climate Change of the Ministry of Education, College of Atmospheric Sciences, Lanzhou University, Lanzhou 730000, China
[b] Collaborative Innovation Center for Western Ecological Safety, Lanzhou University, Lanzhou 730000, China

ARTICLE INFO

Keywords:
Northeast spring precipitation
Dipole mode
Circulation characteristics
Physical mechanism
Numerical experiment

ABSTRACT

Previous studies rarely consider the regional disparity in precipitation variability beyond the overall consistency in Northeast China (NEC). This study examines the spatial distribution and variability of spring precipitation in NEC, a critical region for grain production that is prone to precipitation-related natural disasters. Our results indicate that approximately 26.7% of spring precipitation events in NEC demonstrate a dipole pattern—characterized by contrasting precipitation distributions within the region—that is significantly influenced by low-pressure systems. Our analysis reveals a strong connection between these precipitation patterns and the preceding winter's sea ice conditions in the Kara Sea. Reduced sea ice leads to a decrease in Ural Mountain snow cover, lower surface albedo, and an increase in upward heat flux, thereby warming the lower atmosphere. This process weakens the meridional temperature gradient, slows the westerly jet stream, and intensifies cyclogenesis over NEC. Moreover, persistent anomalies in sea ice and snow cover drive the eastward movement of Rossby waves, shaping the "− + −" Eurasian teleconnection pattern that intensifies regional low-pressure systems. Consequently, these circulation patterns result in increased precipitation in northern NEC and decreased precipitation in the south. Additionally, numerical experiments using the CAM6.0 and LBM model were conducted to investigate the atmospheric response to sea ice loss and the subsequent dynamical mechanisms affecting precipitation in NEC. Therefore, variations in Kara Sea ice and Eurasia snow cover serve as predictive indicators for NEC's spring precipitation pattern, thereby enhancing our understanding of NEC's precipitation dynamics and providing vital insights for predicting and managing regional natural disasters.

1. Introduction

Northeast China (NEC), situated between 38 and 55°N and 110–135°E, located within the East Asian monsoon domain, represents a climate-sensitive zone and a crucial center for industry and agriculture in China. Spring, a crucial growth period for crops, receives less research focus on its precipitation compared to summer. Despite its lower precipitation levels than summer, spring weather and climate in NEC shows unique features distinct from other seasons, exhibiting diverse characteristics across various time scales. Recent research indicates an increasing trend in spring precipitation in NEC (Liang et al., 2011; Zhai et al., 2005), noting that abnormal precipitation patterns can lead to severe natural disasters such as flood or drought, posing significant risks to socioeconomic stability and human safety (Zeng et al., 2019; Zhang et al., 2017a, 2017b; Wang et al., 2024; Zhang et al., 2023a, 2023b). Therefore, examining the climate features and patterns of spring precipitation holds crucial practical implications for harnessing NEC's spring precipitation resources effectively.

Precipitation in the NEC region not only exhibits seasonal variations but also shows distinct spatial differences (Chen et al., 2012; Han et al., 2021; Wang et al., 2019). Various factors including the Arctic Oscillation/North Atlantic Oscillation, Pacific Decadal Oscillation (Wang et al., 2014; Wu and Mao, 2018; He and Wang, 2013; Sun and Yang, 2012; Xiao et al., 2015; Zhu et al., 2023), Equatorial Pacific Sea Surface Temperature (SST) (Stephan et al., 2018; Yang and Lau, 2004; Jing and Sun, 2023; Ren et al., 2019), and Tropical Indian Ocean SST (Yang et al., 2009; Cao et al., 2013; Gao et al., 2014) influence these patterns. Moreover, Eurasian soil moisture (Zhu, 2011), Northeast Cold Vortex

* Corresponding author at: Key Laboratory for Semi-Arid Climate Change of the Ministry of Education, College of Atmospheric Sciences, Lanzhou University, Lanzhou 730000, China.
E-mail address: wangss@lzu.edu.cn (S. Wang).

https://doi.org/10.1016/j.atmosres.2026.108829
Received 22 December 2025; Received in revised form 25 January 2026; Accepted 1 February 2026
Available online 3 February 2026

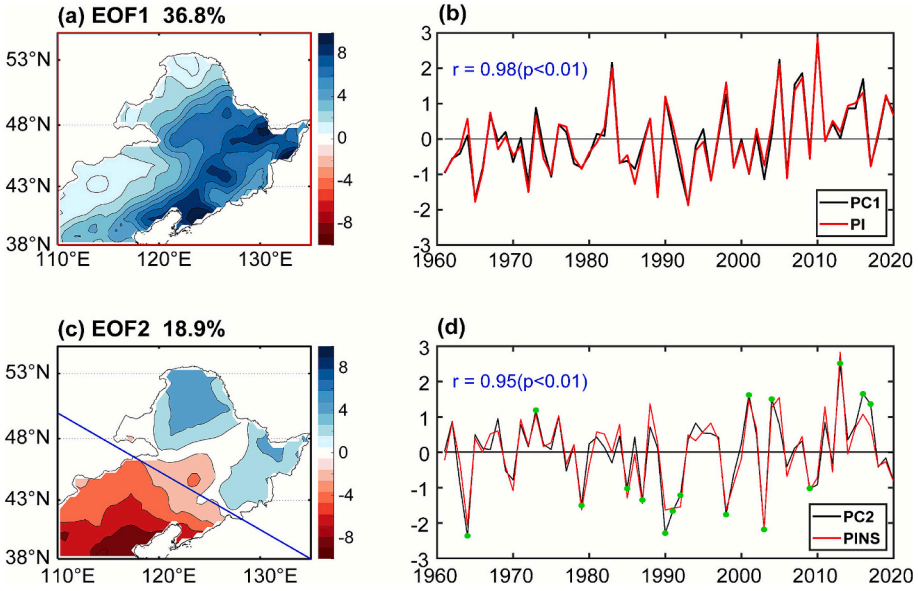

Fig. 1. The (a) spatial pattern and (b) the corresponding standardized time series (PC1, black line) of the first EOF mode (EOF1) of spring precipitation in NEC during 1961–2020. The c, d are the same as a、b, but for the second mode of EOF (EOF2) for spring precipitation in the NEC. The red lines in (b) represent the regional average precipitation (PI) in spring in NEC, and the blue lines in (c) show the dividing line of the precipitation dipole phase. The red lines in (d) indicates the standardized precipitation difference index (PINS) between the north and south regions during the spring in the NEC, and the green dots denote dipole events where | PC2| exceeds one standard deviation. (For interpretation of the references to colour in this figure legend, the reader is referred to the web version of this article.)

Table 1
Definitions of the indices used in this study. All indices have been standardized.

Index	Definition
PI	Calculated through regional averaging of precipitation distance levels in the northeastern region (38–55°N, 110–135°E) during spring.
PINS	The average precipitation anomaly in the northern region (46–55°N, 117–135°E) of the Northeast, minus the average precipitation anomaly in the southern region (38–46°N, 110–128°E) (the blue line in Fig. 1c is the North-South divide).
NECLI	Calculate the average of 500-hpa HGT in the range of 40°-50°N and 120°-130°E multiplied by −1.
EKSICI	The average winter Arctic sea ice extent within the ranges of 74°N to 77°N and 75°E to 85°E, multiplied by −1.
EUSDI	The average winter snow depth in the regions of Eurasia between 65°N to 72°N and 68°E to 82°E, multiplied by −1.

Table 2
The table of phase relationships for all indices presented in this paper. (* means the coefficient values above 95% confidence level, ** means the coefficient values above 99% confidence level).

Index	PINS	NECLI	EKSICI	EUSDI
PC2	0.95**	0.50**	0.29*	0.30*
NECLI	0.45**	/	0.35**	0.32*

Table 3
Experimental designs for CAM6.0.

Name	Resolution	Institute	
CESM (version2.1.3)	Official tag: f09 f09 mg17Atmos: CAM6, 0.9 × 1.25 finite volume grid;192 × 288 lat/lon, 32 vertical-levels	NCAR·&UCAR/USA	
Experiments Name	Experimental design	Duration	Results
Control experiment (CTL)	Forced operation based on observed monthly SIC climate averages (1981–2010 averages)	32 years	LSIC-CTL
Low Sea Ice experiment (LSIC)	Same as CTL, but sea ice values in the Kara Sea (74°-77°N, 75°-85°E) were climatized to −0.5 during the DJF.		

Table 4
Experimental designs for LBM.

Experiment	Center of force	Radius (Lat×Lon)	Extremum (K/day)
EXP_LBM(SIC+SD)	71.0°N, 76.5°E, 850hpa	6.0° × 8.5°	+1.3

(Wu et al., 2022; Lian et al., 2016), as well as the Tibetan Plateau and Eurasian snow cover (Wang and He, 2015; Zuo et al., 2012; Wu and Kirtman, 2007; Zuo et al., 2011) are among the contributing factors. Among them, Zhao et al. (2018) point out that low-pressure systems and anomalous cyclones over the NEC are key factors influencing precipitation in the NEC, and the stronger the Northeast low pressure (NECL), the intensity of the NECL system is directly proportional to the amount of rainfall in the NEC (Cao et al., 2018; Du et al., 2016). Therefore, a follow-up study based on the effect of the NECL system on precipitation in the NEC is conducted in this paper. Furthermore, research indicates that the Eurasian (EU) teleconnection serves as a key low-frequency pattern influencing climate and precipitation variations in the Eurasian continent, particularly impacting NEC given its geographical position (Zhang et al., 2018; Zhang and Wu, 2011; Du et al., 2022). It's important to highlight that this teleconnection pattern strengthens the jet stream over East Asia, deepening the East Asian trough, and consequently affecting both temperature and precipitation patterns in eastern China (Liu et al., 2012). At the same time, Hong and Lu (2016) point out that the Silk Road wave train propagating along the westerly jet in the mid-latitudes would often cause cyclonic anomalies over East Asia. In addition, the Japan-Pacific/East Asia-Pacific teleconnections in the middle and low latitudes also have a certain impact on climate change in Northeast Asia (Zhang et al., 2019a).

Previous studies consistently highlight the significant role of Eurasian snow cover and Arctic sea ice as crucial external drivers

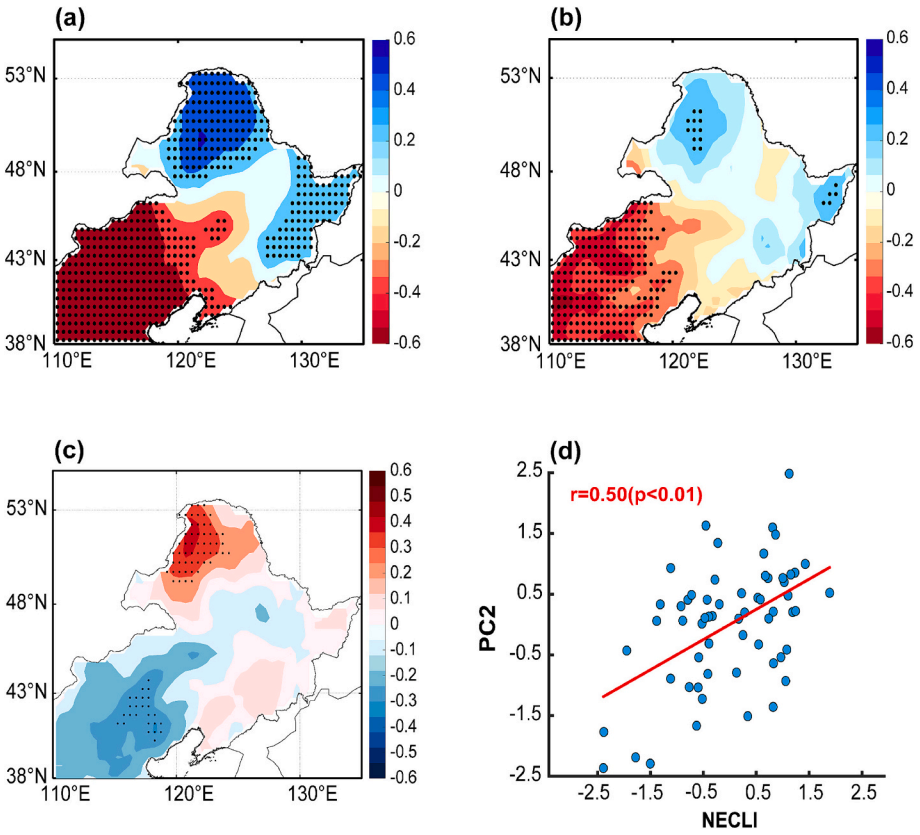

Fig. 2. Spatial distributions of correlation coefficients between spring precipitation in NEC and (a) PC2 and (b) the NECLI, respectively. (c) Correlation between spring precipitation in NEC and the winter EKSICI. (d) Normalized time series of the NECLI and PC2 during the period 1961–2020. Regions that are statistically significant at the 5% level are dotted.

influencing atmospheric variability in the middle to high latitude regions of the Northern Hemisphere. Numerous researches demonstrates that Arctic sea ice anomalies influence East Asian weather and climate patterns through modulation of albedo feedback and regulation of water vapor and energy (Honda et al., 2009; Screen et al., 2018; Lin and Li, 2018; Gao et al., 2015). Recent investigations reveal that the decline in Barents Sea ice cover during June triggers a Rossby wave pattern that propagates eastward, similar to the Silk Road pattern, inducing anomalous meridional circulation over East Asia, which results in anomalous summer precipitation in the region (He et al., 2018a, 2018b). Wu et al. (2016) emphasize how changes in Arctic sea ice trigger anomalous Rossby waves, which strengthen the low-pressure system over the Mongolian Plateau and the subtropical westerly jet stream. This mechanism subsequently enhances spring precipitation in East Asia. Additionally, Arctic sea ice anomalies contribute to meridional temperature gradients between the Arctic and Eurasia, establishing the "warm Arctic-cold Eurasia" pattern. This pattern facilitates the southward transport of Arctic cold air into the Far East, resulting in extreme cold events across the mid to high latitudes of the Northern Hemisphere (Petoukhov and Semenov, 2010; Hu et al., 2018; Yin et al., 2023; Yin et al., 2024; Zhang et al., 2023a, 2023b). Subsequently, this phenomenon influences snow anomalies in Eurasia (Li et al., 2018; Liu et al., 2012) and alters precipitation patterns in East Asia (Yim et al., 2010; Liu and Yanai, 2002; Thackeray et al., 2019; Zhang et al., 2019a, 2019b).

Previous research primarily concentrates on the overall changes in precipitation in NEC, paying less attention to its spatial differences in precipitation distribution (Liang et al., 2011; Lu et al., 2020; Sun and Wang, 2013; Wang and He, 2015). In recent years, however, studies such as those by Han et al. (2019, 2021) begin to highlight a significant dipole pattern in NEC's summer precipitation, revealing a less pronounced decrease in rainfall in the northern areas compared to the southern areas. Furthermore, our recent research (Shu et al., 2024) confirms this distinct north-south precipitation pattern during the summer season. Interestingly, our latest analysis indicates that the distribution of spring precipitation in the NEC is also characterized by a distinct dipole structure, as illustrated in Fig. 1c. This emerging evidence marks a shift in focus from the overall changes in NEC's precipitation to more detailed regional differences, which are crucial for understanding the broader climatic dynamics of the area.

Specifically, this research aims to address three key questions: 1) What are the spatiotemporal patterns of spring precipitation in NEC? 2) What factors contribute to the dipole precipitation pattern observed in this region during the spring season? 3) What physical mechanisms underlie these patterns? By solving these problems, we further study the causes affecting the spring precipitation variability and its spatial distribution in NEC, to provide effective early prediction factors for spring precipitation in NEC, so as to better prevent and reduce natural disasters caused by precipitation.

2. Data and methods

This paper utilizes the daily precipitation grid dataset (version 2.0) provided by the China Meteorological Agency (CMA) and processed by Zhao et al. (2014) using the Thin Plate Spline method for spatial interpolation (Han et al., 2023; Qin et al., 2022). The dataset has a horizontal resolution of 0.5° × 0.5° and spans the period from 1961 to 2020. For the purposes of this study, we convert the data into monthly data usage. We also use the monthly mean ERA5 reanalysis from the European Centre for Medium-Range Weather Forecasts (ECMWF) to calculate the geopotential height, temperature, zonal wind, meridional wind, and vertical velocity. The vertical layers extend from 1000 hPa to 100 hPa, comprising 10 layers, with a horizontal resolution interpolated to 2.5° ×

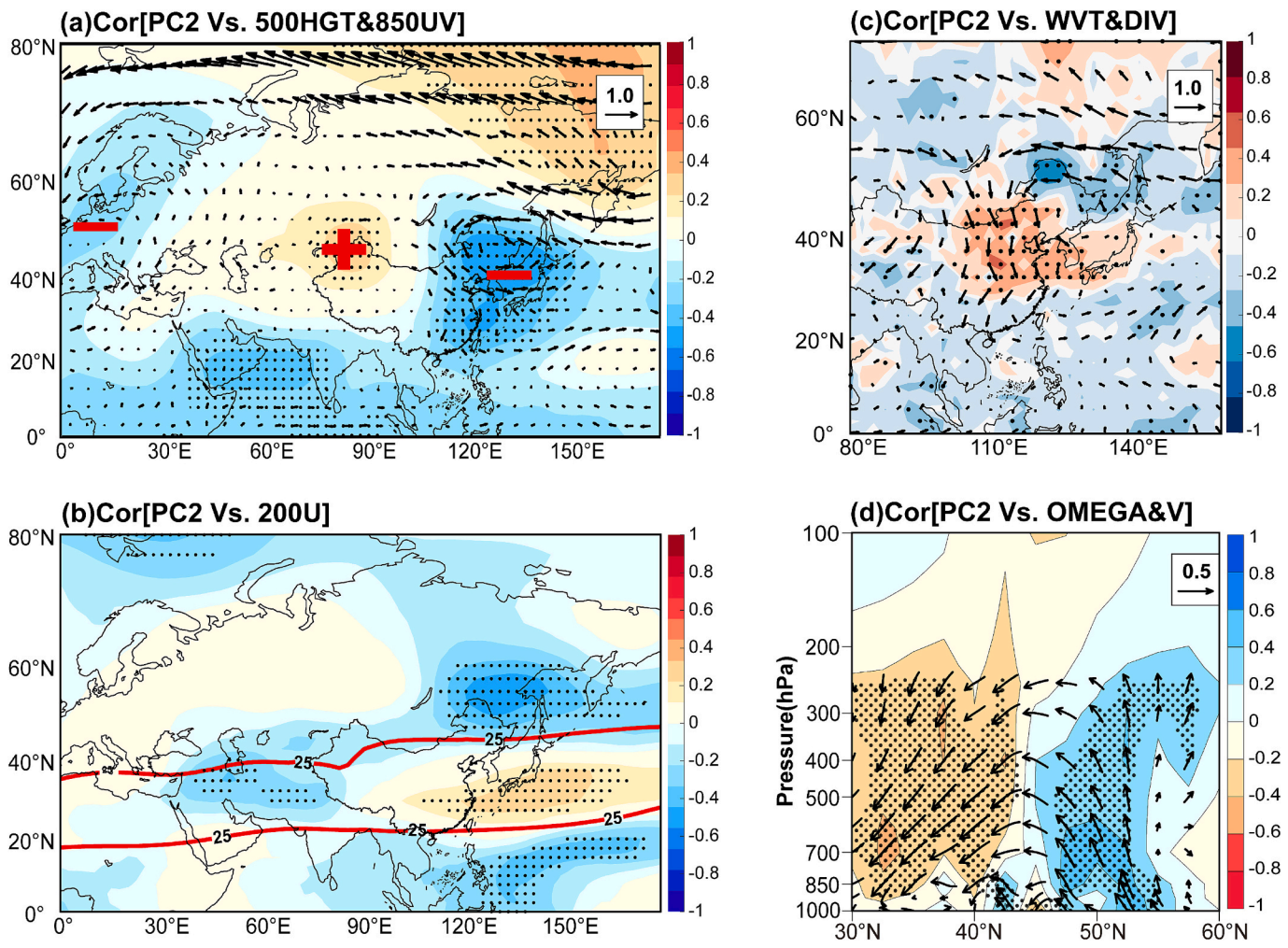

Fig. 3. Correlation coefficients of 500-hPa HGT (a, shading) and 850-hPa horizontal wind vector (a, vectors), 200-hPa U-wind (b), vertical integral of water vapor flux (c, vectors) and divergence (c, shading) in spring with PC2 during 1961–2020. Latitude–height cross section of spring V-wind (d, vector) and Omega (d, shadow) averaged for 110°-135° E correlated with PC2 during the period 1961–2020. The Omega values are multiplied by −100. Positive (negative) moisture flux divergence indicates divergence (convergence). Similarly, a positive (negative) vertical velocity (w) indicates upward (downward) motion. In (a), the "-" indicates the low-pressure center, while the "+" signifies the high-pressure center. The red line in (b) is the climatic westerly jet. Regions that are statistically significant at the 5% level are dotted. (For interpretation of the references to colour in this figure legend, the reader is referred to the web version of this article.)

2.5°. Additionally, ERA5 offers data on surface sensible heat flux and surface latent heat flux, surface albedo, sea ice and the vertical integral of water vapor fluxes and divergence (Hersbach et al., 2020). Furthermore, the selection of snow depth data provided by ERA5 is employed to effectively reflect the change of snow cover across Eurasia at middle and high latitudes (Akyurek et al., 2023; Varga and Breuer, 2023; Muñoz-Sabater et al., 2021; Mortimer et al., 2020). All of the above data cover the period 1961 to 2020. The climate state mean is defined as the 30-year average over the period 1981–2010, and anomalies are computed by subtracting this climate state.

In this study, the precipitation index (PI) for the NEC region is defined as the anomaly calculated from the average precipitation over the entire region (Table 1). The North-South dipole precipitation index (PINS) for the NEC region is defined as the precipitation difference between areas north and south of a demarcated line (Fig. 1c). Winter is defined as the December–January–February (DJF) mean, which includes December of the preceding year and January–February of the current year, and Spring refers to the March–May mean (MAM). In addition, we calculate the Takaya and Nakamura (T-N; Takaya and Nakamura, 2001) wave activity fluxes to describe the propagation conditions of quasi-stationary Rossby waves. We also computed the Eliassen-Palm (*E*-P) flux (Edmon et al., 1980; Andrews, 1987) to characterize the vertical wave propagation involved in stratosphere-troposphere coupling.

In addition, to validate the mechanism of sea ice's impact on spring precipitation dipole pattern in NEC and whether it can serve as a predictive indices for changes in precipitation in NEC, we conduct numerical experiments utilizing the Community Atmosphere Model version 6.0 (CAM6.0) within the framework of the atmosphere component of Community Earth System Model (CESM) version 2.1.3, developed by the National Center for Atmospheric Research (NCAR) (Lauritzen et al., 2018; Danabasoglu et al., 2020). The model operates at a horizontal resolution of 192 latitude × 288 longitude and incorporates 32 hybrid sigma-pressure levels, which are subsequently interpolated to 17 standard pressure levels for analysis. SST is set to a constant climatological state. Building upon this framework, we execute two sets of experiments over a 32-year period (Table 3): a control experiment (CTL) and a low sea ice concentration experiment (LSIC). The CTL simulations utilize forcings derived from monthly sea ice values, which are calculated based on the climatic averages from the period 1981 to 2010. The LSIC experiment is conducted under the same fundamental conditions as the control experiment, with the exception that the sea ice concentration in the Kara Sea (74°–77°N, 75°–85°E) is subtracted by 0.5 from the climate state values during the months of December and February. The

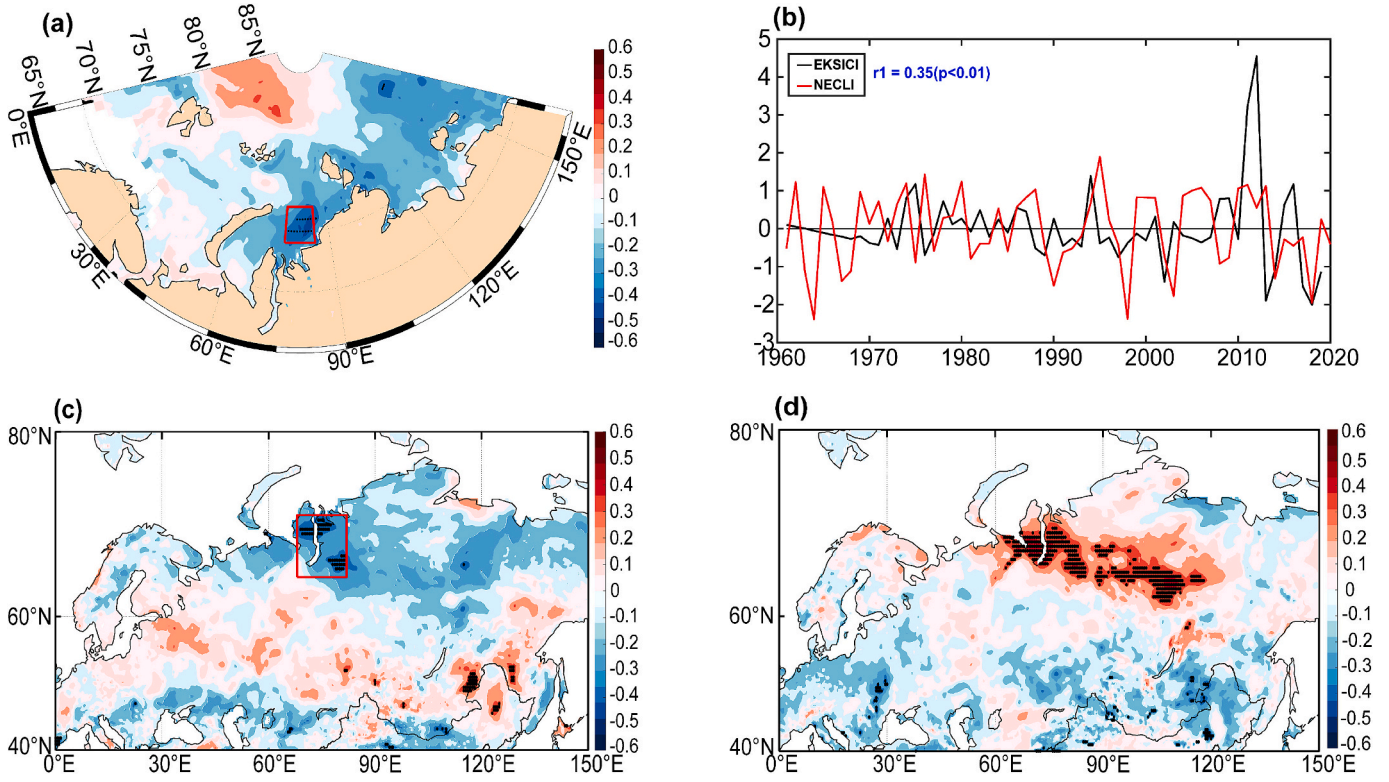

Fig. 4. Correlation coefficients of spring NECLI with pre-winter sea ice (a), pre-winter snow depth (c), and EKSICI with snow depth (d). (b) Time series plot and correlation coefficients of EKSICI versus the NECLI. Regions that are statistically significant at the 1% level are dotted. The red rectangular boxes in (a) and (c) denote critical areas for sea ice and snow depth, respectively. (For interpretation of the references to colour in this figure legend, the reader is referred to the web version of this article.)

simulation results from the last 30 years of both experiments are utilized for analysis. The modeled atmospheric response is defined as the ensemble mean derived by subtracting the ensemble mean of the control run from that of the low sea ice experiment.

To investigate the atmospheric response to diabatic heating resulting from sea ice loss in the Kara Sea, we performed an idealized forcing experiment using the Linear Baroclinic Model (LBM) (Watanabe and Kimoto, 2000). The model was configured with a T42 horizontal resolution and 20 sigma levels in the vertical. The basic state was set to the DJF (December–January–February) climatological mean. An idealized thermal forcing was applied at the lower level over the predefined key region for sea ice and snow (71°N ± 6.0°, 76.5°E ± 8.5°), with a heating rate of approximately 1.3 K day^{-1}. Following a 50-day spin-up, the model output from the final 20 days was used for analysis. For specific experimental details, please refer to Table 4.

3. Results

3.1. Variability and circulation characteristics of spring precipitation in NEC

Many studies show that spring precipitation is on the rise, making it the second most precipitation-rich season of the year after summer (Liang et al., 2011; Yang et al., 2005). To investigate the characteristics of spring precipitation in NEC, we analyze the empirical orthogonal function (EOF) of the spring precipitation anomaly field in the NEC from 1961 to 2020 to obtain the primary modes. The results show that the first mode exhibits a consistent change in precipitation distribution throughout the region, with high values located in the southeast (Fig. 1a). Conversely, the EOF2 mode exhibits a distinct dipole pattern, with opposing precipitation anomalies north and south of a southwest-northeast trending axis spanning 43°–48°N, and the most extreme anomalies located in the northernmost and southernmost parts of the study region (Fig. 1c).The explained variance for this mode is 18.9%. Further analysis reveals that the time series of the above EOF all exhibit significant interannual variability characteristics (Fig. 1b, d, black lines). The correlation coefficient between the principal component of EOF2 (PC2) and the PINS index is 0.95, which is statistically significant at the 1% level ($p < 0.01$) (Table 2).This suggests that a positive value of PC2 corresponds to a mode in which precipitation increases in the northern regions of NEC while decreasing in the southern regions. Conversely, a negative value of PC2 indicates a pattern characterized by increased precipitation in the south and decreased precipitation in the north.

During Spring, we define a NEC dipole precipitation event as occurring when the absolute value of the normalized PC2 exceeds one standard deviation and is greater than that of PC1. Based on this criterion, the frequency of such dipole precipitation events over the past 60 years is approximately 26.7% (Fig. 1d). This indicates that the north-south opposite distribution of precipitation in the NEC region holds a significant proportion. Therefore, investigating the dipole precipitation patterns in spring in NEC is deemed essential. Through analyzing the circulation field associated with PC2, we identify a significant low-pressure center over NEC in spring (Fig. 3a), so we believe that this circulation pattern may affect the occurrence of this anti-phase precipitation pattern in NEC. Therefore, following the method proposed by Liu et al. (2012), we define a Northeast China Low-pressure Index (NECLI) for spring, which is calculated as the average of the areas in the range of 40° -50°N and 120° -130°E of the 500-hpa HGT, multiplied by −1. We use NECLI for the subsequent study of NEC spring precipitation characteristics. The results show that the correlation coefficient between NECLI and PC2 reached 0.5 (significant at the 1% level ($p < 0.01$), Fig. 2c). A larger NECLI value indicates a stronger low-pressure system over NEC, leading to the pattern of wet in the north and dry in the south

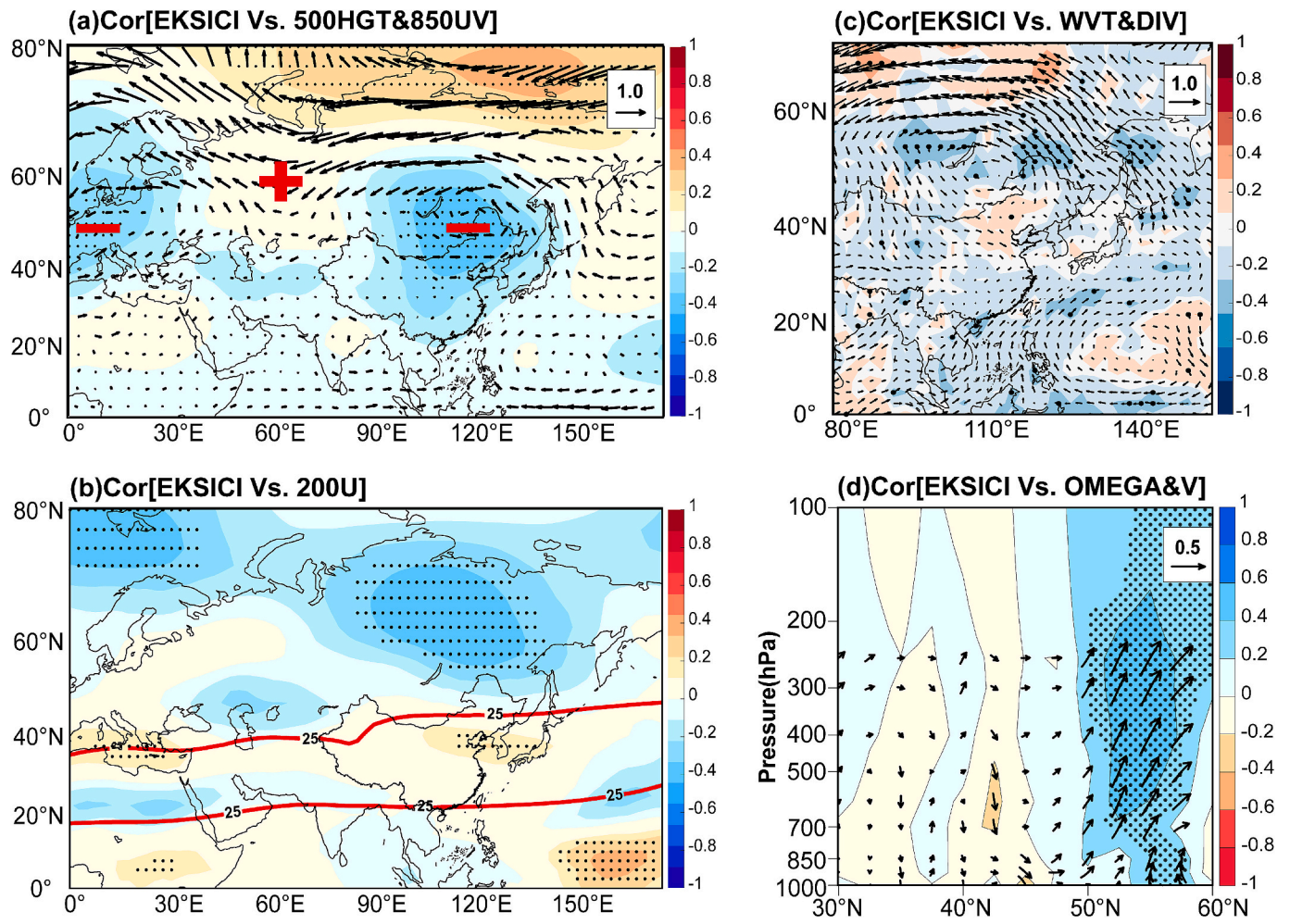

Fig. 5. Correlation coefficients of 500-hPa HGT (a, shading) and 850-hPa horizontal wind vector (a, vectors), 200-hPa U-wind (b), water vapor flux (c, vectors) and divergence (c, shading) in spring with EKSICI during 1961–2020. Latitude–height cross section of spring V-wind (d, vector) and Omega (d, shadow) averaged for 110°-135° E correlated with EKSICI during the period 1961–2020. The Omega values are multiplied by −100. The red line in (b) is the climatic westerly jet. Regions that are statistically significant at the 5% level are dotted. (For interpretation of the references to colour in this figure legend, the reader is referred to the web version of this article.)

increased in NEC (Fig. 2b).

In relation to the dipole-type precipitation pattern observed in spring in NEC, we conduct a correlation analysis between the springtime circulation field and PC2. Illustrated in Fig. 3a is a pronounced "− + −" zonal circulation pattern observed in the 500 hPa height field across the mid to high latitudes of Eurasia. Notably, a significant positive HGT anomaly is present in Central Asia, while a negative HGT anomaly extends from eastern to NEC toward the Sea of Japan. In the corresponding 850 hPa horizontal wind field, NEC is controlled by an anomalous cyclone. The warm and humid easterly wind originating from the North Pacific Ocean leads to significant anomalous upward movement and water vapor flux divergence in the northern part of NEC, which is conducive to increasing precipitation (Fig. 3b, d). Conversely, due to the combination of the cyclone above and the significant high-pressure anomaly in the west, a westerly anomaly appears from the southern NEC to the Yellow Sea. The anomalous northwesterly wind transports dry, cold air from higher latitudes. In the northern part of the region, this cold air converges with warm, moist air advected from the south, forcing the warm, moist air to ascend and generate enhanced precipitation. Meanwhile, over the southern part, the northward diversion of the warm, moist air, coupled with subsidence associated with the dry, cold air, promotes moisture flux divergence and increases atmospheric stability (Fig. 3b-d). This suppresses convective activity, leading to reduced precipitation. This dynamical process establishes a characteristic north-south dipole precipitation pattern, with wetter conditions in the north and drier conditions in the south, which is mechanistically consistent with the spatial pattern shown in Fig. 1c.

3.2. *Possible mechanism of winter sea ice affecting spring precipitation dipole model in NEC*

Arctic sea ice serves as a crucial remote forcing factor influencing the circulation patterns in the mid and high latitudes of Eurasia, thereby playing a pivotal role in regulating subsequent changes in precipitation and temperature in East Asia through its enduring climatic impacts (Liu et al., 2019; Kelleher and Screen, 2017; Li et al., 2018; Hu et al., 2022). Fig. 4a demonstrates a strong negative relationship between the dipole precipitation in the NEC region during spring and the preceding winter's sea ice variations near the Kara Sea. Based on the findings in Fig. 4, we identify the region spanning 74°N to 77°N and 75°E to 85°E as the significant area of sea ice influencing the spring precipitation pattern in NEC. Within this region, we calculate the average sea ice extent and multiply it by −1 to derive the sea ice index (EKSICI). Consequently, higher EKSICI values denote greater sea ice loss. Furthermore, the correlation between EKSICI and NECLI is found to be 0.35, while the correlation coefficient between EKSICI and PC2 is 0.29 (Table 2 and Fig. 4b), which both passed the significance test. This indicates that an increase in sea ice loss is correlated with a more intense low-pressure

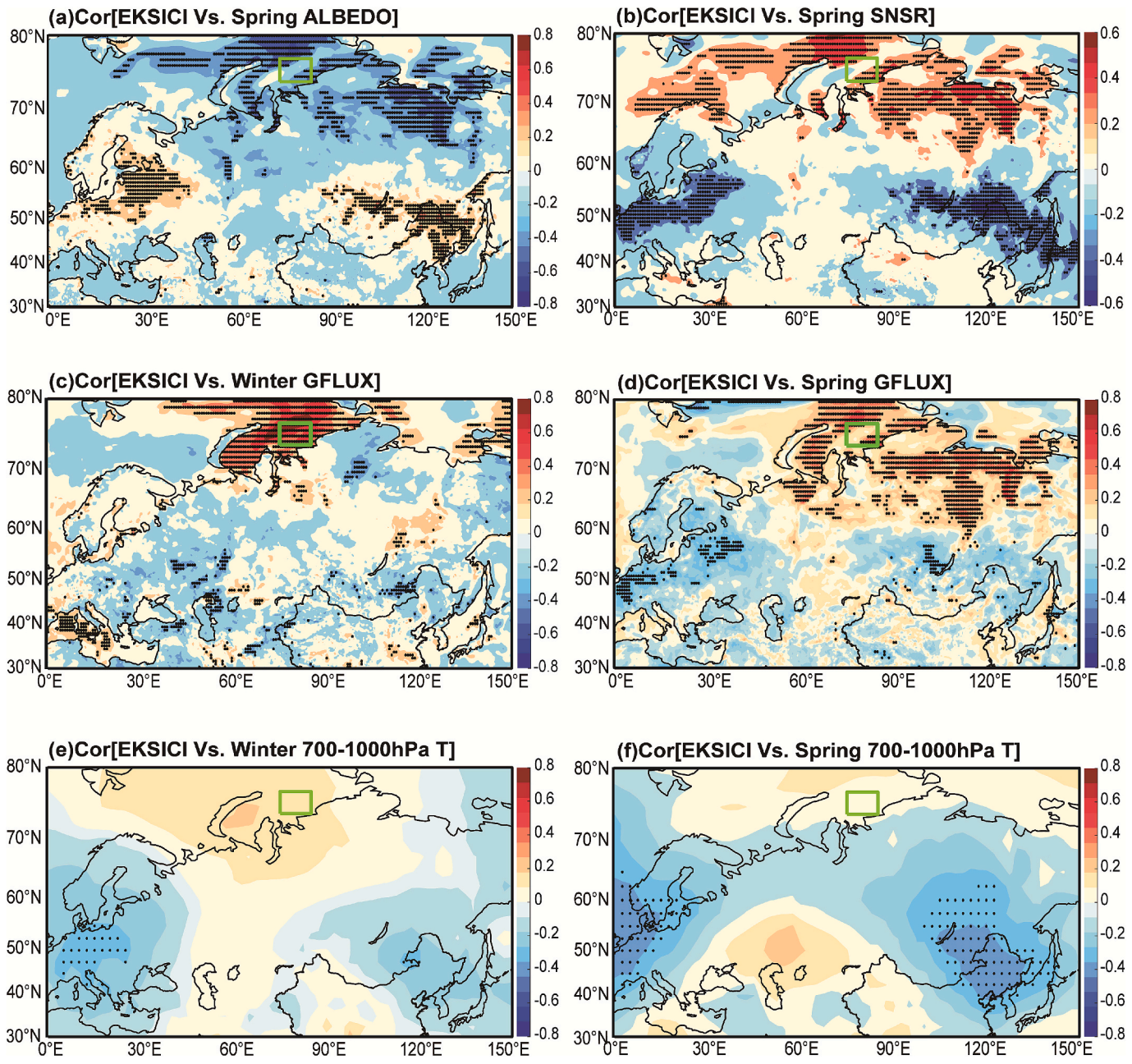

Fig. 6. Spring albedo (a), surface net solar radiation (b), heat flux (d), lower - atmosphere temperature (f, average atmospheric temperature from 700 to 1000-hPa), winter heat flux (c), and winter lower - atmosphere temperature (e, average atmospheric temperature from 700 to 1000-hPa) associated with winter EKSICI. Regions that are statistically significant at the 5% level are dotted. The key sea - ice region is outlined by a green rectangle. (For interpretation of the references to colour in this figure legend, the reader is referred to the web version of this article.)

system over the NEC, leading to enhanced precipitation in the northern regions and a reduction in precipitation in the southern areas of the NEC during the spring (Fig. 2c).This indicates that greater sea ice loss is correlated with a more intense low-pressure system over the NEC, leading to enhanced precipitation in the northern regions and a reduction in precipitation in the southern areas of the NEC during the spring (Fig. 2a-b). In addition to Kara Sea ice, the snow cover over Eurasia also plays a significant role in influencing the variability of climate in mid-high latitudes (Zhang et al., 2021a, 2021b; Handorf et al., 2015; Zuo et al., 2012; Saito et al., 2001). Previously, Zhang et al. (2022b) point out that the anomalous reductions of the Barents- Kara Sea ice during the previous winter is not only significantly correlated with the snow water equivalent of the east-west dipole pattern in Eurasian continent but also significantly linked to springtime precipitation in Northeast Asia on an interannual scale. Consequently, we perform a correlation analysis between pre-winter snow cover and NECLI, as illustrated in Fig. 4c, revealing a negative correlation between snow cover in the northern part of the Eurasian continent and the dipole precipitation pattern. We select the area of significance (65 to 72°N, 68 to 82°E, red rectangular box) and calculated the area-averaged snow cover index (EUSDI) by multiplying it with −1. This indicates that when the snow depth east of the Ural Mountains and the Kara Sea ice in the previous winter show negative anomalies, the precipitation in the north of NEC increases, while the precipitation in the south decreases in the spring.

To investigate how sea ice anomalies influence the spring dipole precipitation patterns in NEC, we examine the atmospheric circulation anomalies linked to EKSICI. Our findings reveal that reduced sea ice cover near the Kara Sea in the pre-winter could leads to positive HGT

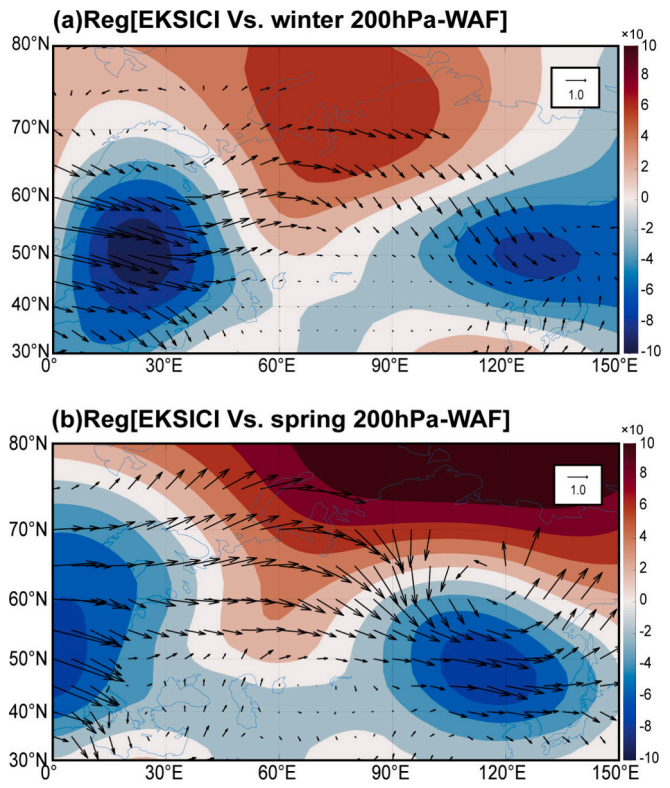

Fig. 7. The regression of winter (a) and spring (b) 200-hpa HGT anomaly (shading, gpm) and wave flux (T-N, vector, m^2s^{-2}) with preceding winter EKSICI.

anomalies in the upper atmosphere over the relevant areas and negative anomalies over the Lake Baikal to NEC region (Fig. 5a), which is consistent with the PC2 related circulation pattern in Fig. 3a. This atmospheric configuration generates a wave train across the mid-to-high latitudes of Eurasia that exhibits a structure similar to the EU teleconnection pattern (characterized by a "– + –" anomaly pattern). The persistence of this EU-like circulation pattern helps maintain and intensify the low-pressure system over NEC (Zhang et al., 2018). Additionally, anomalous cyclonic circulation prevails in the 850 hPa wind field over the NEC region, with notably strong southeast winds in the north. These intense southeast winds transport warm, moist air from the ocean to the NEC, enhancing the convergence of water vapor flux and upward motion. As a result, this facilitates increased precipitation in the northern areas (Fig. 5c, d). On the contrary, the positive zonal wind anomaly and subsidence in the south suppressed the precipitation.

Furthermore, upon examining the mechanism through which snow cover impacts spring precipitation in NEC, we observe similarities between the circulation patterns and influencing mechanisms associated with the EUSDI and those linked to sea ice affecting precipitation (Fig. S1, S2 and Figs. 5, 6). In addition, we investigate the correlation between sea ice and snow cover and find a significant positive relationship between the two key areas (Fig. 4d), with an index correlation coefficient of 0.38 between the two key areas. Consequently, we believe that the combined effects of Kara sea ice and the snow cover in the eastern Urals contribute to the north-south opposite pattern of spring precipitation in the NEC. In general, a decrease in Arctic sea ice is anticipated to result in decreased snow cover across northern Eurasia, leading to enhanced spring rainfall in the northern and decreased precipitation in the southern parts of the NEC.

The complex interactions between sea ice and atmospheric circulation often involve mechanisms such as albedo and surface heat flux (Curry et al., 1995; Budikova, 2009; Vihma, 2014; Gao et al., 2015). As illustrated in Fig. 6a, the reduction of Kara Sea ice in the preceding winter lowers surface albedo and enhances the absorption of shortwave solar radiation. Simultaneously, the expansion of open water suppresses the escape of outgoing longwave radiation to the atmosphere, further amplifying heat accumulation at the surface and in the lower atmosphere. This net warming effect, driven by both shortwave and longwave radiation processes, raises surface temperature and strengthens upward sensible and latent heat fluxes. Through enhanced ocean–atmosphere heat exchange, more energy is transferred into the atmosphere, leading to elevated air temperatures in the lower Arctic troposphere (Fig. 6e–f). The heating of the earth to the atmosphere increases the thickness of the atmosphere, resulting in a geopotential height anomaly in the vicinity of the Kara Sea and across the Arctic region (Ye et al., 2024; Chatterjee et al., 2023; Jiang et al., 2024). However, sea ice reduction persists from the previous winter to the subsequent spring (correlation $r = 0.29$, Fig. S3a - c). The resultant thermal anomaly heats the lower - troposphere atmosphere and transfers upward to the lower stratosphere through the tropopause (Fig. S4a - b), warming the stratosphere. This upward heat flux can alter the stratospheric bottom temperature structure and upward - propagating wave energy (Xu et al., 2023; Sellevold et al., 2016; Cohen et al., 2020; Screen and Francis, 2016), affecting the stratospheric circulation pattern (Fig. S4c, e). These signals persist in the stratosphere into the following spring (Fig. S4e-f; Baldwin et al., 2003), with downward-extending energy emerging in the lower-to-middle troposphere, inducing corresponding responses within the mid-high latitude tropospheric atmosphere (Fig. S4d - f) (Wu et al., 2016; Wu and Smith, 2016; Nakamura et al., 2016; Zhang et al., 2022b; Xu et al., 2020; Cohen and Agel, 2021; Sun et al., 2015; Screen and Francis, 2016; McKenna and Bracegirdle, 2018). Persistent vertical thermal anomalies in the atmosphere can induce a baroclinic response in the lower troposphere (Overland et al., 2015; Honda et al., 2009; Inoue et al., 2012). This favors the excitation of Rossby waves. However, the weakened westerlies slow their eastward propagation during winter and spring. Consequently, a latitudinal wave train pattern resembling a Eurasian teleconnection (" -+- ") is established over Western Europe extending to the Ural Mountains (Liu et al., 2014), and subsequently propagates across the mid to high latitudes toward Northeast Asia (Fig. 7). Anomalous easterly winds generated by anticyclones in the northern upper troposphere enhance the transport of cold advection, leading to the southward movement of cold air from northern regions into the Far East (Honda et al., 2009; Mori et al., 2019).

Furthermore, the warming associated with the loss of sea ice is detrimental to the formation and persistence of snow cover (Fig. S3d-f). The increase in lower atmospheric temperatures likely corresponds with a decline in snow cover around the Ural Mountains (Zhang et al., 2022b; Hezel et al., 2012; Park et al., 2013). The reduction in snow cover further contributes to a decrease in surface albedo, which in turn results in elevated temperatures at high latitudes (Mu and Zhou, 2012; Brown et al., 2010). In addition, the hydrological effect of snow cover also affects surface processes and atmospheric circulation (Yasunari et al., 1991; Barnett et al., 1989; Xu and Dirmeyer, 2011; Xu and Dirmeyer, 2013a, 2013b). The snow cover in northern Eurasia gradually melts with the increase in temperature from winter to the following spring. As shown in Fig. S2 and Fig. S5, both reduced albedo and increased soil moisture resulting from diminished snow cover trigger persistent anomalies in upward heat flux and wave activity flux propagation (Zhang et al., 2017a, 2017b; Halder and Dirmeyer, 2017; Xu et al., 2021; Sun et al., 2021). This phenomenon establishes a positive feedback loop, which promotes the propagation of the Rossby wave train (Fig. S2d). The combined action of the snow cover's albedo effect and the delayed hydrological effects gives rise to Arctic warming. These anomalous signals modulate springtime mid-to-high latitude circulation patterns over Eurasia by influencing stratospheric circulation anomalies and subsequent stratosphere-troposphere coupling (Fig. S6). Simultaneously, accompanied by the cooling in the mid - latitudes of Eurasia, this situation decreases the atmospheric thickness gradient as well as the meridional temperature gradient from the Arctic to Eurasia. The

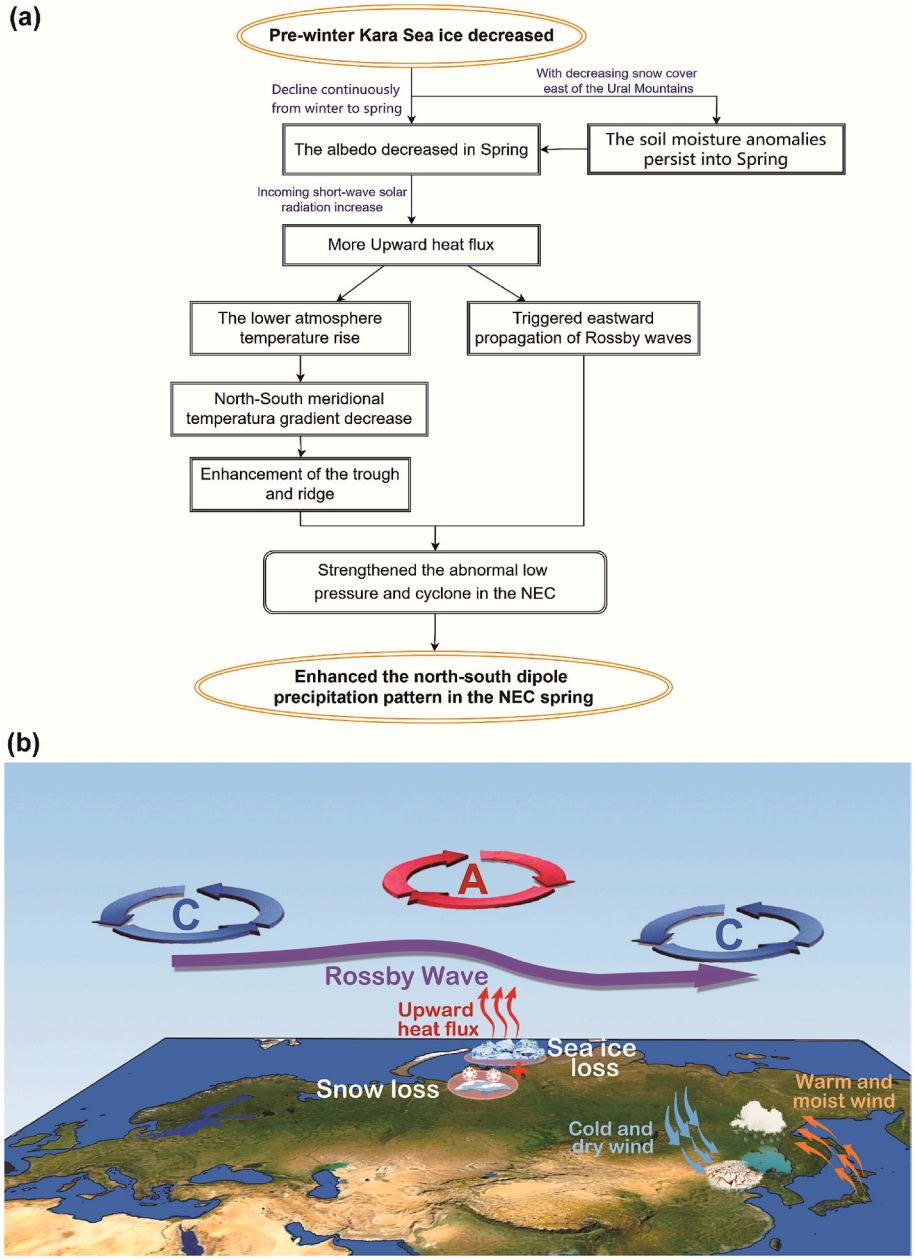

Fig. 8. (a) The physical mechanism chain and (b) schematic diagram illustrating the impact of Arctic sea ice on the spring precipitation dipole pattern in the NEC. In the figures, "A" denotes an anticyclone, and "C" denotes a cyclone. The areas circled in pink are key areas for sea ice and snow cover. (For interpretation of the references to colour in this figure legend, the reader is referred to the web version of this article.)

warming of the Arctic, coupled with cooling in mid-latitude Eurasia, reduces both the atmospheric thickness gradient and the meridional temperature gradient from the Arctic to Eurasia. This weakens the westerly jet, deepening the trough and ridge pattern from Siberia to Northeast Asia (Ding et al., 2021; Petrie et al., 2015; Chen et al., 2020; Sellevold et al., 2016; Francis and Vavrus, 2012), which in turn intensifies low pressure and cyclonic activity over Lake Baikal and the NEC. Ultimately, the winter disappearance of Kara Sea ice affects high-latitude Eurasian snow melting by interacting with atmospheric circulation. This leads to the convergence of cold air and low-pressure anomalies from the Arctic over the NEC, enhancing the North-South dipole precipitation pattern. Fig. 8 illustrates this mechanism.

3.3. Results from CAM6.0 and LBM experiments

To better understand and validate the mechanisms by which sea ice influences precipitation in Northeast China, we conducted idealized adiabatic heating forcing experiments using a Linear Baroclinic Model (LBM) and sensitivity experiments with the Community Atmosphere Model (CAM6.0). The model results successfully reproduce the previously observed atmospheric and precipitation anomalies over the Arctic and Eurasia in spring following winter sea ice anomalies. As shown in Fig. 9a–d, the models accurately replicate the observed processes: winter sea ice loss in the Kara Sea leads to reduced spring snow cover over northern Eurasia, which subsequently increases soil moisture due to snowmelt. Simultaneously, the reduction in sea ice cover decreases surface albedo, enhancing the absorption of solar radiation. These two processes collectively strengthen upward heat fluxes from winter to spring, warming the overlying atmosphere into the stratosphere. Furthermore, the idealized adiabatic heating experiments with the LBM demonstrate that Kara Sea ice loss generates thermal forcing that excites anomalous upward wave activity flux propagating eastward. These

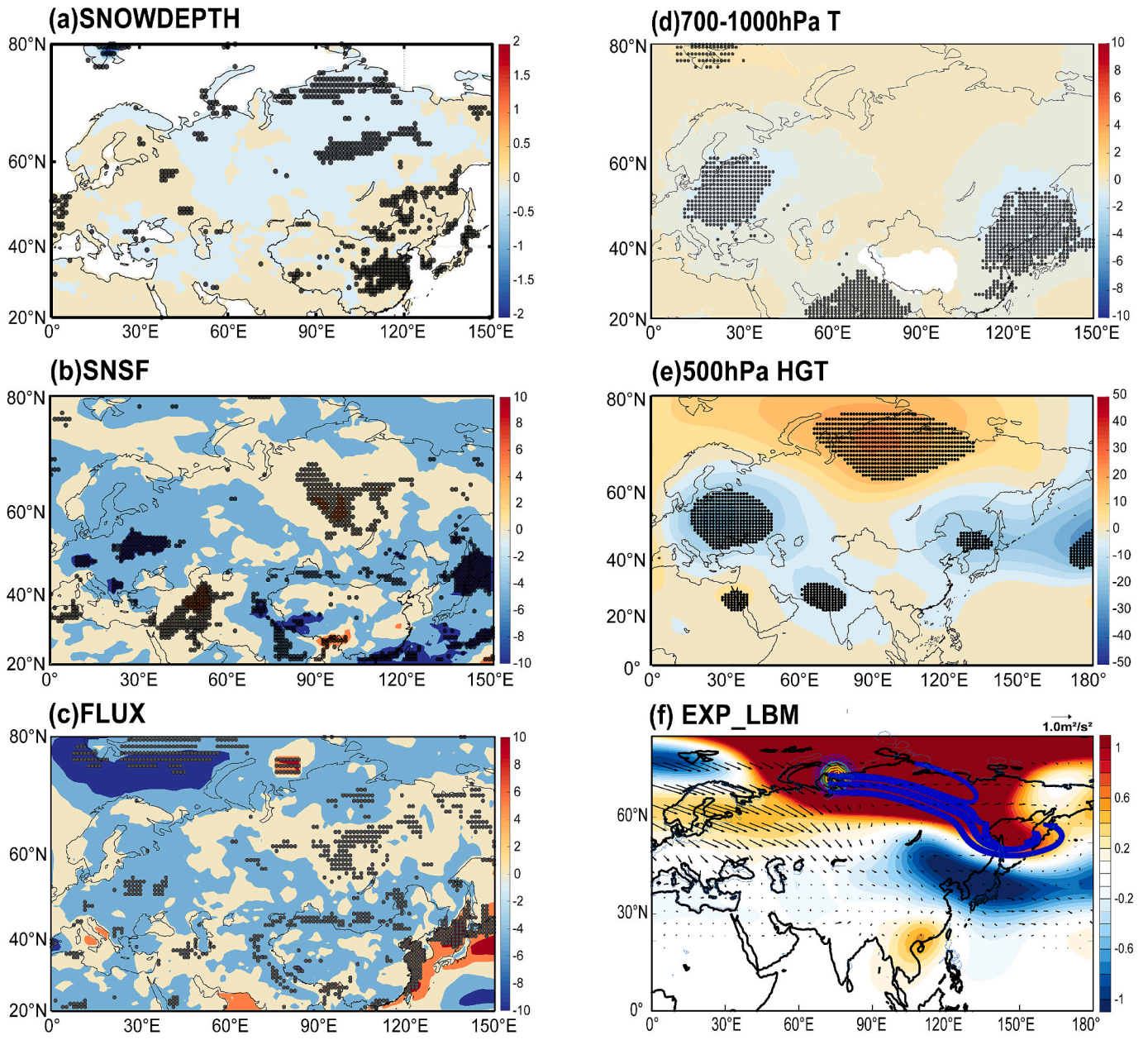

Fig. 9. Composite differences in (a) snow-depth (units: m), (b) net surface solar radiation (units: W/m^2), (c) surface heat flux (units: W/m^2), (d)700–1000-hPa mean air temperature (contour, units: °K), (e) 500-hPa geopotential height (units: m) for MAM between the control and Low Sea Ice experiments based on CAM6 (LSIC-CTL). (f) The 500-hPa geopotential height (shading; m) averaged over the last 20 days of the LBM ensemble simulation, with the blue curve showing the wavenumber-1 Rossby wave ray path at day 11. Vectors represent the composite difference in spring 500-hPa horizontal Takaya–Nakamura wave activity flux (m^2 s^{-2}) from the CAM6 experiment. Dotted areas denote statistical significance at the 10% level. (For interpretation of the references to colour in this figure legend, the reader is referred to the web version of this article.)

anomalous thermal and geopotential height signals persist into the following spring via the stratospheric memory effect. Concurrently, atmospheric warming over the Arctic weakens the meridional temperature gradient between the polar and subtropical regions. The resulting deceleration of the westerly jet stream slows the eastward propagation of Rossby waves. Consequently, a west–east oriented Rossby wave train pattern ("– + –") forms and persists over Eurasia from winter to spring (Fig. 9e–f), consistent with the 110-year model results of Xia et al. (2024). This wave train thereby fosters the development of an anomalous cyclonic circulation over Northeast Asia. This circulation provides a dynamical disturbance background conducive to precipitation, which in turn reinforces the dipole tendency in regional rainfall distribution (Fig. S7b).

Simulated outcomes align well with observational evidence, lending support to the role of winter Kara Sea ice anomalies in shaping the north–south dipole mode of spring precipitation over NEC. The simulations confirm that reduced sea ice forces large-scale circulation, exciting a Rossby wave train that extends from the polar region to the mid-latitudes and establishes a pronounced upper-level cyclonic anomaly over NEC. This dynamical disturbance provides a key background condition that polarizes the spatial distribution of precipitation, thereby promoting the formation of the dipole precipitation pattern over Northeast Asia in spring. These findings validate the physical mechanism illustrated in Fig. 8.

4. Conclusions and discussions

This study delves into the interannual variability of spring precipitation in NEC spanning 1961–2020, exploring its primary influencing factors and associated mechanisms. The spatial characteristics of spring rainfall in NEC demonstrate a pronounced dipole distribution, with the north being wet and the south being dry. The corresponding principal component (PC2) exhibits significant interannual variability. Over the last six decades, this dipole precipitation pattern accounts for about 32% of the total precipitation model. This implies that precipitation trends in NEC evolve beyond uniform changes to encompass a distinct north-south inverse phase pattern. Hence, there is a pressing need for deeper exploration and analysis of the regional nuances in precipitation variability within NEC.

Our findings suggest that the spring dipole precipitation pattern observed in the NEC is significantly affected by low-pressure systems, which are primarily influenced by the pre-winter sea ice conditions in the Kara Sea and the snow cover east of the Ural Mountains. Furthermore, a significant correlation exists between sea ice and snow cover in these regions, and the physical mechanism by which both influence spring precipitation in the NEC are similar (Zhang and Sun, 2020; Zhang et al., 2020; Zhang et al., 2022b; Zhang et al., 2022a; Wu et al., 2016). The reduction of sea ice in the Kara Sea during the preceding winter likely diminished snow cover in northern Eurasia, causing a decrease in surface albedo and an increase in upward heat flux. Such variations in surface thermal forcing may induce anomalous upward wave activity flux, exciting eastward-propagating Rossby waves that manifest as a "− + −" zonal wave train over Eurasia, somewhat like the EU teleconnection. This wave train subsequently induces a quasi-stationary cyclonic anomaly over NEC, deepening the local low-pressure center. Simultaneously, the increased surface heat flux warms the lower atmosphere at high latitudes. This warming effect over the Arctic is likely to weaken the meridional temperature gradient in the middle and high latitudes of Eurasia, weakening the westerly winds. As a result, this process deepens the troughs and ridges and intensifies anomalous cyclones over the NEC. Anomalous cyclones and low-pressure centers contribute to heightened water vapor divergence and descending movement anomalies in the southern region of NEC, while the opposite effect occurs in the northern part, leading to a distinct dipole pattern characterized by dry conditions in the south and wet conditions in the north. Furthermore, we conduct sensitivity experiments using CAM6.0, which demonstrate that the loss of sea ice in the pre-winter Kara Sea influences circulation changes through a positive feedback mechanism arising from the interaction between anomalous thermal conditions and the atmosphere (Mori et al., 2014; Cho et al., 2022). This interaction yields an atmospheric circulation pattern akin to the Eurasian teleconnection observed in the mid to high latitudes of Eurasia (Liu et al., 2014; Xu et al., 2019, 2022; Wang et al., 2024).

This study examines the influence of interannual sea ice and snow cover variations on spring precipitation patterns in NEC. Numerical experiments demonstrate that winter Kara Sea ice loss triggers an atmospheric teleconnection wave train that affects subsequent spring climate. However, NEC precipitation is modulated by multiple factors, including North Atlantic SSTs, Eurasian snow water equivalent, and soil moisture over the Tibetan Plateau and Yangtze Basin (Zuo and Zhang, 2007; Zuo et al., 2012; Zuo and Zhang, 2016). Decadal-scale variations in warm pool and Indian Ocean SSTs further underscore the importance of low-frequency climate signals (Yang and Lau, 2004; Chen et al., 2014; Lu et al., 2020). Mid-latitude circulation patterns such as the NAO and AO regulate cold-air activity by modulating the Ural blocking and East Asian trough (Ding et al., 2021; Park et al., 2013). The position and intensity of the NEC cold vortex also critically shape precipitation distributions (Xu et al., 2023; Xie and Bueh, 2015; Xu and Qi, 2023; Xue and Zhang, 2022). Recent studies indicate that Arctic sea ice decline induces Eurasian snow cover and soil moisture anomalies that influence NEC spring precipitation (Du et al., 2022; Ji and Fan, 2019). However, internal variability in Arctic sea ice remains a key uncertainty (Ding et al., 2017, 2019), while the observed snow cover decline over northern Eurasia (Ye et al., 2015) and its teleconnections with southern China precipitation (Jia et al., 2018) highlight the need for a more comprehensive understanding of these complex interactions. Given the uneven spatial and temporal distribution of spring precipitation in NEC, which leads to extreme drought, flood and other natural disasters, enhancing the accuracy of spring precipitation forecasts in NEC is paramount. Future research should focus on refining our understanding through detailed numerical experiments, considering both the spatial and temporal distribution of spring precipitation and the external forcing factors that influence these patterns. This comprehensive approach is crucial for managing the risks associated with adverse weather conditions effectively.

CRediT authorship contribution statement

Xinya Shu: Writing – review & editing, Writing – original draft. **Shanshan Wang:** Funding acquisition, Formal analysis. **Yuanyuan Hu:** Conceptualization. **Yiwei Pang:** Data curation. **Hao Wang:** Investigation. **Yongli He:** Methodology. **Fei Ji:** Resources. **Jianping Huang:** Validation. **Jinxia Zhang:** Resources.

Declaration of competing interest

The authors declare that they have no competing financial interests or personal relationships that could influence the work reported in this paper.

Acknowledgments

This work was jointly supported by the National Science Foundation of China (42522503 and 42475023). In particular, the calculation was supported by the Supercomputing Center of Lanzhou University.

Appendix A. Supplementary data

Supplementary data to this article can be found online at https://doi.org/10.1016/j.atmosres.2026.108829.

Data availability

ERA5 reanalysis data are available from https://cds.climate.copernicus.eu/cdsapp#!/dataset/reanalysis-era5-single-levels-monthly-means?tab=form. The NCEP–NCAR reanalysis dataset is available at https://psl.noaa.gov/data/reanalysis/reanalysis.shtml. Precipitation observations were obtained from https://data.cma.cn/site/showSubject/id/46.html, which is the data set of gridded daily precipitation in China (Version 2.0) (SURF_CLI_CHN_PRE_DAY_GRID_0.5.txt) provided by the National Meteorological Information Center of China Meteorological Administration (NMIC/CMA). Due to the data policy in China, these data records are currently not available via a website for public download. However, researchers could contact the China Meteorological Data Service Center (http://www.cma.gov.cn/en2014/aboutcma/contactus/) for detailed information on data acquisition. The CAM6.0 model can be downloaded from http://github.com/ESCOMP/CESM.Figures in this manuscript were made with MATLAB version 2020a and this software is available from www.mathworks.com/ (The Math Works, Inc., 2020).

References

Akyurek, Z., Kuter, S., Karaman, Ç.H., Akpınar, B., 2023. Understanding the snow cover climatology over Turkey from ERA5-Land reanalysis data and MODIS snow cover frequency product. Geosciences 13 (10), 311. https://doi.org/10.3390/geosciences13100311.

Andrews, D.G., 1987. On the interpretation of the eliassen-palm flux divergence. Q.J.R. Meteorol. Soc. 113, 323–338. https://doi.org/10.1002/qj.49711347518.
Baldwin, M.P., Stephenson, D.B., Thompson, D.W.J., Dunkerton, T.J., Charlton, A.J., O'Neill, A., 2003. Stratospheric memory and skill of extended-range weather forecasts. Science 301, 636–640. https://doi.org/10.1126/science.1087143.
Barnett, T.P., Dümenil, L., Schlese, U., et al., 1989. The effect of Eurasian snow cover on regional and global climate variations. J. Atmos. Sci. 46, 661–686. https://doi.org/10.1175/1520-0469(1989)046<0661:TEOESC>2.0.CO;2.
Brown, R., Derksen, C., Wang, L., 2010. A multi-data set analysis of variability and change in Arctic spring snow cover extent, 1967–2008. J. Geophys. Res. 115, D16111. https://doi.org/10.1029/2010JD013975.
Budikova, D., 2009. Role of Arctic Sea ice in global atmospheric circulation: a review. Glob. Planet. Chang. 68, 149–163. https://doi.org/10.1016/j.gloplacha.2009.04.001.
Cao, J., Lu, R., Hu, J., Wang, H., 2013. Spring Indian Ocean–western Pacific SST contrast and the East Asian summer rainfall anomaly. Adv. Atmos. Sci. 30, 1560–1568. https://doi.org/10.1007/s00376-013-2298-6.
Cao, F., Gao, T., Dan, L., Ma, Z., Yang, X., Yang, F., 2018. Contribution of large-scale circulation anomalies to variability of summer precipitation extremes in Northeast China. Atmos. Sci. Lett. 19, e867. https://doi.org/10.1002/asl.867.
Chatterjee, S., Selivanova, J., Semmler, T., Screen, J.A., 2023. Ocean response to reduced Arctic Sea ice in PAMIP simulations. In: EGU General Assembly Conference Abstracts (pp. EGU-4822). https://doi.org/10.5194/egusphere-egu23-4822.
Chen, H.P., Sun, J.Q., Fan, K., 2012. Decadal features of heavy rainfall events in eastern China. J. Meteorol. Res. 26, 289–303. https://doi.org/10.1007/s13351-012-0303-0.
Chen, J.P., Wen, Z.P., Wu, R., Chen, Z.S., Zhao, P., 2014. Interdecadal changes in the relationship between southern China winter–spring precipitation and ENSO. Clim. Dyn. 43, 1327–1338. https://doi.org/10.1007/s00382-013-1947-x.
Chen, D., Gao, Y., Sun, J., Wang, H., Ma, J., 2020. Interdecadal variation and causes of drought in Northeast China in recent decades. J. Geophys. Res. Atmos. 125, e2019JD032069. https://doi.org/10.1029/2019JD032069.
Cho, H., Kug, J.S., Jun, S.Y., 2022. Influence of the recent winter Arctic Sea ice loss in short-term simulations of a regional atmospheric model. Sci. Rep. 12, 8901. https://doi.org/10.1038/s41598-022-12783-4.
Cohen, J., Agel, L., 2021. Barlow, M., Garfinkel, C. I. & White, I. Linking Arctic variability and change with extreme winter weather in the United States. Science 373, 1116–1121. https://doi.org/10.1126/science.abi9167.
Cohen, J., et al., 2020. Divergent consensuses on Arctic amplification influence on midlatitude severe winter weather. Nat. Clim. Chang. 10, 20–29. https://doi.org/10.1038/s41558-019-0662-y.
Curry, J.A., Schramm, J.L., Ebert, E.E., 1995. Sea ice–albedo climate feedback mechanism. J. Clim. 8, 240–247. https://doi.org/10.1175/1520-0442(1995)008<0240:SIACFM>2.0.CO;2.
Danabasoglu, G., Lamarque, J.-F., Bacmeister, J., Bailey, D.A., DuVivier, A.K., Edwards, J., et al., 2020. The Community Earth System Model Version 2 (CESM2). Journal of Advances in Modeling Earth Systems 12, e2019MS001916. https://doi.org/10.1029/2019MS001916.
Ding, S., Wu, B., Chen, W., 2021. Dominant Characteristics of early Autumn Arctic Sea Ice Variability and its Impact on Winter Eurasian climate. J. Clim. 34, 1825–1846. https://doi.org/10.1175/JCLI-D-19-0834.1.
Du, M.X., Lin, Z.D., Lu, R.Y., 2016. Inter-decadal change in the summertime Northeast Asia low-pressure system in the early 1990s. J. Atmos. Sci. 40, 805–816 (in Chinese). https://doi.org/10.3878/j.issn.1006-9895.1511.15178.
Du, Y., Zhang, J., Zhao, S., et al., 2022. A mechanism of spring Barents Sea ice effect on the extreme summer droughts in northeastern China. Clim. Dyn. 58, 1033–1048. https://doi.org/10.1007/s00382-021-05949-9.
Edmon, H.J., Hoskins, B.J., McIntyre, M.E., 1980. Eliassen-Palm Cross Sections for the Troposphere. J. Atmos. Sci. 37, 2600–2616. https://doi.org/10.1175/1520-0469(1980)037<2600:EPCSFT>2.0.CO;2.
Francis, J.A., Vavrus, S.J., 2012. Evidence linking Arctic amplification to extreme weather in mid-latitudes. Geophys. Res. Lett. 39, L06801. https://doi.org/10.1029/2012GL051000.
Gao, Z., Hu, Z., Zhu, J., Yang, S., Zhang, R., Xiao, Z., Jha, B., 2014. Variability of Summer Rainfall in Northeast China and its connection with Spring Rainfall Variability in the Huang-Huai Region and Indian Ocean SST. J. Clim. 27, 7086–7101. https://doi.org/10.1175/JCLI-D-14-00217.1.
Gao, Y., Sun, J., Li, F., et al., 2015. Arctic Sea ice and Eurasian climate: a review. Adv. Atmos. Sci. 32, 92–114. https://doi.org/10.1007/s00376-014-0009-6.
Halder, S., Dirmeyer, P.A., 2017. Relation of Eurasian snow cover and Indian summer monsoon rainfall: Importance of the delayed hydrological effect. J. Clim. 30 (4), 1273–1289. https://doi.org/10.1175/JCLI-D-16-0033.1.
Han, T., He, S., Wang, H., et al., 2019. Variation in principal Modes of Midsummer Precipitation over Northeast China and its Associated Atmospheric Circulation. Adv. Atmos. Sci. 36, 55–64. https://doi.org/10.1007/s00376-018-8072-z.
Han, T., Zhang, M., Zhu, J., et al., 2021. Impact of early spring sea ice in Barents Sea on midsummer rainfall distribution at Northeast China. J Climate Dynamics 57, 1023–1037. https://doi.org/10.1007/s00382-021-05754-4.
Han, J., Miao, C., Gou, J., Zheng, H., Zhang, Q., Guo, X., 2023. A new daily gridded precipitation dataset for the Chinese mainland based on gauge observations. Earth Syst. Sci. Data 15, 3147–3161. https://doi.org/10.5194/essd-15-3147-2023.
Handorf, D., Jaiser, R., Dethloff, K., Rinke, A., Cohen, J., 2015. Impacts of Arctic Sea ice and continental snow cover changes on atmospheric winter teleconnections. Geophys. Res. Lett. 42, 2367–2377. https://doi.org/10.1002/2015GL063203.
He, S., Wang, H., 2013. Impact of the November/December Arctic Oscillation on the following January temperature in East Asia. J. Geophys. Res. Atmos. 118, 12,981–12,988. https://doi.org/10.1002/2013JD020525.
He, S., Gao, Y., Furevik, T., et al., 2018a. Teleconnection between sea ice in the Barents Sea in June and the Silk Road, Pacific–Japan and East Asian rainfall patterns in August. Adv. Atmos. Sci. 35, 52–64. https://doi.org/10.1007/s00376-017-7029-y.
He, C., Lin, A., Gu, D., et al., 2018b. Using eddy geopotential height to measure the western North Pacific subtropical high in a warming climate. Theor. Appl. Climatol. 131, 681–691. https://doi.org/10.1007/s00704-016-2001-9.
Hersbach, H., Bell, B., Berrisford, P., Hirahara, S., Horányi, A., Muñoz-Sabater, J., et al., 2020. The ERA5 global reanalysis. Q. J. R. Meteorol. Soc. 146 (730), 1999–2049. https://doi.org/10.1002/qj.3803.
Hezel, P.J., Zhang, X., Bitz, C.M., Kelly, B.P., Massonnet, F., 2012. Projected decline in spring snow depth on Arctic Sea ice caused by progressively later autumn open ocean freeze-up this century. Geophys. Res. Lett. 39, L17505. https://doi.org/10.1029/2012GL052794.
Honda, M., Inoue, J., Yamane, S., 2009. Influence of low Arctic Sea, ice minima on anomalously cold Eurasian winters. Geophys. Res. Lett. 36, L08707. https://doi.org/10.1029/2008GL037079.
Hong, X., Lu, R., 2016. The Meridional Displacement of the Summer Asian Jet, Silk Road Pattern, and Tropical SST Anomalies. J. Clim. 29, 3753–3766. https://doi.org/10.1175/JCLI-D-15-0541.1.
Hu, X., Cai, M., Yang, S., Sejas, S., 2018. Air temperature feedback and its contribution to global warming. Sci. China Earth Sci. 61, 1491–1509. https://doi.org/10.1007/s11430-017-9226-6.
Hu, X., Liu, Y., Kong, Y., Yang, Q., 2022. A quantitative analysis of the source of inter-model spread in Arctic surface warming response to increased CO2 concentration. Geophys. Res. Lett. 49, e2022GL100034. https://doi.org/10.1029/2022GL100034.
Inoue, J., Hori, M.E., Takaya, K., 2012. The Role of Barents Sea Ice in the Wintertime Cyclone Track and Emergence of a Warm-Arctic Cold-Siberian Anomaly. J. Clim. 25, 2561–2568. https://doi.org/10.1175/JCLI-D-11-00449.1.
Ji, L., Fan, K., 2019. Interannual linkage between wintertime sea-ice cover variability over the Barents Sea and springtime vegetation over Eurasia. Clim. Dyn. 53, 5637–5652. https://doi.org/10.1007/s00382-019-04884-0.
Jia, X., Cao, D.R., Ge, J.W., Wang, M., 2018. Interdecadal change of the impact of Eurasian snow on spring precipitation over southern China. J. Geophys. Res. Atmos. 123, 10,092–10,108. https://doi.org/10.1029/2018JD028612.
Jiang, J., He, S., Fan, K., 2024. Recent impact of reduced arctic sea-ice on the winter North Atlantic jet stream and its quantitative contributions compared to pre-industrial level. Atmos. Res., 107778 https://doi.org/10.1016/j.atmosres.2024.107778.
Jing, H., Sun, J., 2023. Diverse impacts of strong and moderate intense El Niño–Southern Oscillation events on spring precipitation over Asia. Int. J. Climatol. 43 (13), 6300–6313. https://doi.org/10.1002/joc.8206.
Kelleher, M., Screen, J., 2017. Atmospheric precursors of and response to anomalous Arctic Sea ice in CMIP5 models. Adv. Atmos. Sci. 35, 27–37. https://doi.org/10.1007/s00376-017-7039-9.
Lauritzen, P.H., Nair, R.D., Herrington, A.R., Callaghan, P., Goldhaber, S., Dennis, J.M., et al., 2018. NCAR release of CAM-SE in CESM2.0: a reformulation of the spectral element dynamical core in dry-mass vertical coordinates with comprehensive treatment of condensates and energy. Journal of Advances in Modeling Earth Systems 10, 1537–1570. https://doi.org/10.1029/2017MS001257.
Li, H., Chen, H., Wang, H., Sun, J., Ma, J., 2018. Can Barents Sea Ice Decline in Spring Enhance Summer Hot Drought events over Northeastern China? J. Clim. 31, 4705–4725. https://doi.org/10.1175/JCLI-D-17-0429.1.
Lian, Y., Shen, B., Li, S., et al., 2016. Mechanisms for the formation of Northeast China cold vortex and its activities and impacts: an overview. J. Meteorol. Res. 30, 881–896. https://doi.org/10.1007/s13351-016-6003-4.
Liang, L., Li, L., Liu, Q., 2011. Precipitation variability in Northeast China from 1961 to 2008. J. Hydrol. 404 (1–2), 67–76. https://doi.org/10.1016/j.jhydrol.2011.04.020.
Lin, Z.D., Li, F., 2018. Impact of interannual variations of spring sea ice in the Barents Sea on East Asian rainfall in June. Atmos Oceanic Sci Lett 11, 275–281. https://doi.org/10.1080/16742834.2018.1454249.
Liu, X., Yanai, M., 2002. Influence of Eurasian spring snow cover on Asian summer rainfall. Int. J. Climatol. 22, 1075–1089. https://doi.org/10.1002/joc.784.
Liu, J.P., Curry, J.A., Wang, H.J., Song, M.R., Horton, R.M., 2012. Impact of declining Arctic Sea ice on winter snowfall. Proc. Natl. Acad. Sci. 109 (11), 4074–4079. https://doi.org/10.1073/pnas.1114910109.
Liu, Y., Wang, L., Zhou, W., et al., 2014. Three Eurasian teleconnection patterns: spatial structures, temporal variability, and associated winter climate anomalies. Clim. Dyn. 42, 2817–2839. https://doi.org/10.1007/s00382-014-2163-z.
Liu, G., Xu, S.Q., Lian, Y., 2019. Recognition results of blocking high in Asia during summer and its possible impacts on climate anomalies in Northeast China: Comparison of various reanalysis data. Acta. Meteor. Sin. 77 (2), 303–314. https://doi.org/10.11676/qxxb2019.007.
Lu, R., Zhu, Z., Li, T., Zhang, H., 2020. Interannual and Interdecadal Variabilities of Spring Rainfall over Northeast China and their Associated Sea Surface Temperature Anomaly Forcings. J. Clim. 33, 1423–1435. https://doi.org/10.1175/JCLI-D-19-0302.1.
McKenna, C.M., Bracegirdle, T.J., 2018. Shuckburgh, E. F., Haynes, P. H. & Joshi, M. M. Arctic Sea ice loss in different regions leads to contrasting Northern Hemisphere impacts. Geophys. Res. Lett. 45, 945–954. https://doi.org/10.1002/2017GL076433.
Mori, M., Watanabe, M., Shiogama, H., et al., 2014. Robust Arctic Sea-ice influence on the frequent Eurasian cold winters in past decades. Nat. Geosci. 7, 869–873. https://doi.org/10.1038/ngeo2277.
Mori, M., Kosaka, Y., Watanabe, M., Nakamura, H., Kimoto, M., 2019. A reconciled estimate of the influence of Arctic Sea-ice loss on recent Eurasian cooling. Nat. Clim. Chang. 9, 123–129. https://doi.org/10.1038/s41558-018-0379-3.

Mortimer, C., Mudryk, L., Derksen, C., Luojus, K., Brown, R., Kelly, R., Tedesco, M., 2020. Evaluation of long-term Northern Hemisphere snow water equivalent products. Cryosphere 14 (5), 1579–1594. https://doi.org/10.5194/tc-14-1579-2020.

Mu, S.N., Zhou, G.Q., 2012. Mechanism for the correlation of winter fresh snow extent over Northern Eurasia and summer climate anomalies in China: Anomalous seasonal transition of land as a bond (in Chinese). Chin. J. Atmos. Sci. 36, 297–315.

Muñoz-Sabater, J., Dutra, E., Agustí-Panareda, A., Albergel, C., Arduini, G., Balsamo, G., Thépaut, J.N., 2021. ERA5-Land: a state-of-the-art global reanalysis dataset for land applications. Earth Syst. Sci. Data 13 (9), 4349–4383. https://doi.org/10.5194/essd-13-4349-2021.

Nakamura, T., Yamazaki, K., Iwamoto, K., Honda, M., Miyoshi, Y., Ogawa, Y., Tomikawa, Y., Ukita, J., 2016. The stratospheric pathway for Arctic impacts on midlatitude climate. Geophys. Res. Lett. https://doi.org/10.1002/2016GL068330 (2016GL068330).

Overland, J., Francis, J.A., Hall, R., Hanna, E., Kim, S., Vihma, T., 2015. The Melting Arctic and Midlatitude Weather patterns: are they Connected? J. Clim. 28, 7917–7932. https://doi.org/10.1175/JCLI-D-14-00822.1.

Park, H., Walsh, J.E., Kim, Y., Nakai, T., Ohata, T., 2013. The role of declining Arctic Sea ice in recent decreasing terrestrial Arctic snow depths. Polar Sci. 7 (2), 174–187. https://doi.org/10.1016/j.polar.2012.10.002.

Petoukhov, V., Semenov, V.A., 2010. A link between reduced Barents-Kara Sea ice and cold winter extremes over northern continents. J. Geophys. Res. Atmos. 115, D21111. https://doi.org/10.1029/2009JD013568.

Petrie, R.E., Shaffrey, L.C., Sutton, R.T., 2015. Atmospheric response in summer linked to recent Arctic Sea ice loss. Q.J.R. Meteorol. Soc. 141, 2070–2076. https://doi.org/10.1002/qj.2502.

Qin, R., Zhao, Z., Xu, J., Ye, J.-S., Li, F.-M., Zhang, F., 2022. HRLT: a high-resolution (1 d, 1 km) and long-term (1961–2019) gridded dataset for surface temperature and precipitation across China. Earth Syst. Sci. Data 14, 4793–4810. https://doi.org/10.5194/essd-14-4793-2022.

Ren, H.L., Scaife, A.A., Dunstone, N., et al., 2019. Seasonal predictability of winter ENSO types in operational dynamical model predictions. Clim. Dyn. 52, 3869–3890. https://doi.org/10.1007/s00382-018-4366-1.

Saito, K., Cohen, J., Entekhabi, D., 2001. Evolution of Atmospheric Response to Early-season Eurasian Snow Cover Anomalies. Mon. Weather Rev. 129, 2746–2760. https://doi.org/10.1175/1520-0493(2001)129<2746:EOARTE>2.0.CO;2.

Screen, J.A., Francis, J.A., 2016. Contribution of sea-ice loss to Arctic amplification is regulated by Pacific Ocean decadal variability. Nat. Clim. Chang. 6, 856. https://doi.org/10.1038/nclimate3011.

Screen, J.A., et al., 2018. Consistency and discrepancy in the atmospheric response to Arctic Sea-ice loss across climate models. Nat. Geosci. 11, 155–163. https://doi.org/10.1038/s41561-018-0059-y.

Sellevold, R., Sobolowski, S., Li, C., 2016. Investigating possible Arctic-midlatitude teleconnections in a linear framework. J. Clim. 29 (20), 7329–7343. https://doi.org/10.1175/Jcli-D-15-0902.1.

Shu, X., Wang, S., Wang, H., et al., 2024. South-North dipole in summer precipitation over Northeast China. Clim. Dyn. 1-18. https://doi.org/10.1007/s00382-024-07256-5.

Stephan, C.C., Klingaman, N.P., Vidale, P.L., et al., 2018. A comprehensive analysis of coherent rainfall patterns in China and potential drivers. Part I: Interannual variability. Clim. Dyn. 50, 4405–4424. https://doi.org/10.1007/s00382-017-3882-8.

Sun, B., Wang, H.J., 2013. Water Vapor Transport Paths and Accumulation during Widespread Snowfall events in Northeastern China. J. Clim. 26, 4550–4566. https://doi.org/10.1175/JCLI-D-12-00300.1.

Sun, C., Yang, S., 2012. Persistent severe drought in southern China during winter–spring 2011: Large-scale circulation patterns and possible impacting factors. J. Geophys. Res. 117, D10112. https://doi.org/10.1029/2012JD017500.

Sun, L., Deser, C., Tomas, R.A., 2015. Mechanisms of stratospheric and tropospheric circulation response to projected Arctic Sea ice loss. J. Clim. 28, 7824–7845. https://doi.org/10.1175/JCLI-D-15-0169.1.

Sun, Y., Chen, H., Zhu, S., Zhang, J., Wei, J., 2021. Influence of the Eurasian Spring Snowmelt on Summer Land Surface Warming over Northeast Asia and its Associated Mechanism. J. Clim. 34 (12), 1–65. https://doi.org/10.1175/JCLI-D-20-0756.1.

Takaya, K., Nakamura, H., 2001. A Formulation of a Phase-Independent Wave-activity Flux for Stationary and Migratory Quasigeostrophic Eddies on a Zonally varying Basic Flow. J. Atmos. Sci. 58, 608–627. https://doi.org/10.1175/1520-0469(2001)058<0608:AFOAPI>2.0.CO;2.

Thackeray, C.W., Derksen, C., Fletcher, C.G., et al., 2019. Snow and climate: Feedbacks, Drivers, and Indices of Change. Curr. Clim. Chang. Rep. 5, 322–333. https://doi.org/10.1007/s40641-019-00143-w.

Varga, Á.J., Breuer, H., 2023. Evaluation of snow depth from multiple observation-based, reanalysis, and regional climate model datasets over a low-altitude central European region. Theor. Appl. Climatol. 153, 1393–1409. https://doi.org/10.1007/s00704-023-04539-5.

Vihma, T., 2014. Effects of Arctic Sea ice decline on weather and climate: a review. Surv. Geophys. 35, 1175–1214. https://doi.org/10.1007/s10712-014-9284-0.

Wang, H.J., He, S.P., 2015. The North China/Northeastern Asia Severe Summer Drought in 2014. J. Clim. 28, 6667–6681. https://doi.org/10.1175/JCLI-D-15-0202.1.

Wang, S., Huang, J., He, Y., Guan, Y., 2014. Combined effects of the Pacific Decadal Oscillation and El Niño-Southern Oscillation on Global Land Dry–Wet Changes. Sci. Report. 4. https://doi.org/10.1038/srep06651.

Wang, Jian, Gui, Shu, Ma, Anqi, Yang, Ruowen, Zhang, Qi, 2019. Interdecadal Variability of Summer Precipitation Efficiency in East Asia. Adv. Meteorol. 1, 3563024. https://doi.org/10.1155/2019/3563024.

Wang, H., Wang, S., Shu, X., He, Y., Huang, J., 2024. Increasing occurrence of sudden turns from drought to flood over China. J. Geophys. Res. Atmos. 129 (3), e2023JD039974. https://doi.org/10.1029/2023JD039974.

Watanabe, M., Kimoto, M., 2000. Atmosphere-ocean thermal coupling in the North Atlantic: a positive feedback. Q. J. R. Meteorol. Soc. 126, 3343–3369. https://doi.org/10.1002/qj.49712657017.

Wu, R., Kirtman, B.P., 2007. Observed Relationship of Spring and Summer East Asian Rainfall with Winter and Spring Eurasian Snow. J. Clim. 20, 1285–1304. https://doi.org/10.1175/JCLI4068.1.

Wu, X., Mao, J., 2018. Spatial and interannual variations of spring rainfall over eastern China in association with PDO–ENSO events. Theor. Appl. Climatol. 134, 935–953. https://doi.org/10.1007/s00704-017-2323-2.

Wu, Y., Smith, K.L., 2016. Response of northern hemisphere midlatitude circulation to arctic amplification in a simple atmospheric general circulation model. J. Clim. https://doi.org/10.1175/JCLI-D-15-0602.1.

Wu, Z.X., Li, Y., Li, Y., 2016. Potential Influence of Arctic Sea Ice to the Interannual Variations of East Asian Spring Precipitation. J. Clim. 29, 2797–2813. https://doi.org/10.1175/JCLI-D-15-0128.1.

Wu, J., Liu, Y., Li, Y.S., Zuo, J.Q., et al., 2022. The extreme Northeast China Cold Vortex activities in the late spring of 2021 and possible causes involved. Adv. Clim. Chang. Res. 13 (6), 787–796. https://doi.org/10.1016/j.accre.2022.09.002.

Xia, X., Zhang, J., Xu, M., et al., 2024. Impacts of early-winter Arctic Sea-ice loss on wintertime surface temperature in China. Clim. Dyn. 62, 6579–6597. https://doi.org/10.1007/s00382-024-07225-y.

Xiao, M.Z., Zhang, Q., Singh, V.P., 2015. Influences of ENSO, NAO, IOD and PDO on seasonal precipitation regimes in the Yangtze River basin, China. Int. J. Climatol. 35 (12), 3556–3567. https://doi.org/10.1002/joc.4228.

Xie, Z., Bueh, C., 2015. Different Types of Cold Vortex Circulations over Northeast China and their Weather Impacts. Mon. Weather Rev. 143, 845–863. https://doi.org/10.1175/MWR-D-14-00192.1.

Xu, L., Dirmeyer, P., 2011. Snow–atmosphere coupling strength in a global atmospheric model. Geophys. Res. Lett. 38, L13401. https://doi.org/10.1029/2011GL048049.

Xu, L., Dirmeyer, P., 2013a. Snow–atmosphere coupling strength. Part I: effect of model biases. J. Hydrometeorol. 14, 389–403. https://doi.org/10.1175/JHM-D-11-0102.1.

Xu, L., Dirmeyer, P., 2013b. Snow–atmosphere coupling strength. Part II: Albedo effect versus hydrological effect. J. Hydrometeorol. 14, 404–418. https://doi.org/10.1175/JHM-D-11-0103.1.

Xu, S., Qi, L., 2023. Critical influence of the Northeast cold vortex in different positions on precipitation. Clim. Dyn. 60, 867–881. https://doi.org/10.1007/s00382-022-06365-3doi:10.1175/JCLI-D-20-0205.1.

Xu, P., Wang, L., Chen, W., 2019. The British–Baikal Corridor: A Teleconnection Pattern along the Summertime Polar Front Jet over Eurasia. J. Clim. 32, 877–896. https://doi.org/10.1175/JCLI-D-18-0343.1.

Xu, M., Tian, W., Zhang, J., 2020. Wang, T. & Qie, K. Impact of Barents-Kara-Sea sea ice reduction on the variation of east Asian trough in late winter. J. Clim. 34, 1081–1097. https://doi.org/10.1175/JCLI-D-20-0205.1.

Xu, B., Chen, H., Gao, C., Zeng, G., Huang, Q., 2021. Abnormal change in spring snowmelt over Eurasia and its linkage to East Asian summer monsoon: the hydrological effect of snow cover. Front. Earth Sci. 8, 594546. https://doi.org/10.3389/FEART.2020.594656.

Xu, P., Wang, L., Dong, Z., Li, Y., Shen, X., Chen, W., 2022. The British–Okhotsk Corridor Pattern and Its Linkage to the Silk Road Pattern. J. Clim. 35, 5787–5804. https://doi.org/10.1175/JCLI-D-21-0705.1.

Xu, M., Tian, W., Zhang, J., et al., 2023. Important role of stratosphere-troposphere coupling in the Arctic mid-to-upper tropospheric warming in response to sea-ice loss. npj Clim Atmos Sci 6, 9. https://doi.org/10.1038/s41612-023-00333-2.

Xue, D., Zhang, Y., 2022. Wang, P. Et al. Distinct influences of cold vortex over Northeast China on local precipitation in early summer and midsummer. Clim. Dyn. 59, 3701–3716. https://doi.org/10.1007/s00382-022-06291-4.

Yang, F., Lau, K.-M., 2004. Trend and variability of China precipitation in spring and summer: Linkage to sea-surface temperatures. Int. J. Climatol. 24, 1625–1644. https://doi.org/10.1002/joc.1094.

Yang, S., Sun, F., Chen, Y., 2005. Climatic feature spring precipitation anomalies in Northeast China in the past 45 years [in Chinese]. J. Nanjing Insti. Meteorol. 28 (2), 197–204. https://doi.org/10.1007/s10409-004-0010-x.

Yang, J., Liu, Q., Liu, Z., Wu, L., Huang, F., 2009. Basin mode of Indian Ocean Sea surface temperature and Northern Hemisphere circumglobal teleconnection. Geophys. Res. Lett. 36, L19705. https://doi.org/10.1029/2009GL039559.

Yasunari, T., Kitoh, A., Tokioka, T., 1991. Local and remote responses to excessive snow mass over Eurasia appearing in the northern spring and summer climate. J. Meteor. Soc. Japan 69, 473–487. https://doi.org/10.2151/jmsj1965.69.4_473.

Ye, K., Wu, R., Liu, Y., 2015. Interdecadal change of Eurasian snow, surface temperature, and atmospheric circulation in the late 1980s. J. Geophys. Res. Atmos. 120, 2738–2753. https://doi.org/10.1002/2015JD023148.

Ye, K., Woollings, T., Sparrow, S.N., et al., 2024. Response of winter climate and extreme weather to projected Arctic Sea-ice loss in very large-ensemble climate model simulations. npj Clim Atmos Sci. 7, 20. https://doi.org/10.1038/s41612-023-00562-5.

Yim, S.Y., Jhun, J.G., Lu, R., Wang, B., 2010. Two distinct patterns of spring Eurasian snow cover anomaly and their impacts on the East Asian summer monsoon. J. Geophys. Res. Atmos. 115 (D22). https://doi.org/10.1029/2010JD013996.

Yin, Z.C., et al., 2023. Subseasonal variability and the "Arctic warming-Eurasia cooling" trend. Sci. Bull. 68, 528–535. https://doi.org/10.1016/j.scib.2023.02.009.

Yin, Z., Zhang, Y., He, S., et al., 2024. Warm Arctic-Cold Eurasia pattern helps predict spring wildfire burned area in West Siberia. Nat. Commun. 15, 9041. https://doi.org/10.1038/s41467-024-53470-4.

Zeng, D.W., Yuan, X., Roundy, J.K., 2019. Effect of teleconnected land–atmosphere coupling on Northeast China persistent drought in spring–summer of 2017. J. Clim. 32, 7403–7420. https://doi.org/10.1175/JCLI-D-19-0175.1.

Zhai, P., Zhang, X., Wan, H., Pan, X., 2005. Trends in total precipitation and frequency of daily precipitation extremes over China. J. Clim. 18, 1096–1108. https://doi.org/10.1175/JCLI-3318.1.

Zhang, M., Sun, J., 2020. Increased role of late winter sea surface temperature variability over northern tropical Atlantic in spring precipitation prediction over Northeast China. J. Geophys. Res. Atmos. 125, e2020JD033232. https://doi.org/10.1029/2020JD033232.

Zhang, R.N., Wu, B.Y., 2011. The Northern Hemisphere atmospheric response to spring Arctic Sea ice anomalies in CAM3. 0 model. Chin. J. Atmos. Sci. 35, 847–862. https://doi.org/10.3878/j.issn.1006-9895.2011.05.05.

Zhang, Y., Zhang, L., Wang, S.P., Feng, J., 2017a. Drought events and their influence in summer of 2017 in China. J. Arid Meteorol. 35, 899–905 (in Chinese). 10 11755 /j.issn.1006-7639(2017)-05-0899.

Zhang, R., Zhang, R., Zuo, Z., 2017b. Impact of Eurasian spring snow decrement on East Asian summer precipitation. J. Clim. 30 (9), 3421–3437. https://doi.org/10.1175/JCLI-D-16-0214.1.

Zhang, R.N., Sun, C.H., Li, W.J., 2018. The relationship between Arctic Sea ice and summer Eurasian Teleconnection type interannual variation and its influence on summer precipitation in China. (in Chinese). Chin. J. Geophys. 61 (1), 91–105. https://doi.org/10.6038/cjg2018K0755.

Zhang, J., Chen, H., Zhao, S., 2019a. A Tripole Pattern of Summertime Rainfall and the Teleconnections linking Northern China to the Indian Subcontinent. J. Clim. 32, 3637–3653. https://doi.org/10.1175/JCLI-D-18-0659.1.

Zhang, R., Sun, C., Zhang, R., Li, W., Zuo, J., 2019b. Role of Eurasian snow cover in linking winter-spring Eurasian coldness to the autumn Arctic Sea ice retreat. J. Geophys. Res. Atmos. 124, 9205–9221. https://doi.org/10.1029/2019JD030339.

Zhang, R., Sun, C., Zhu, J., et al., 2020. Increased European heat waves in recent decades in response to shrinking Arctic Sea ice and Eurasian snow cover. Npj. Clim. Atmos. Sci. 3, 7. https://doi.org/10.1038/s41612-020-0110-8.

Zhang, D., Huang, Y., Zhou, B., Wang, H., 2021a. Is there Interdecadal Variation in the South Asian High? J. Clim. 34, 8089–W8103. https://doi.org/10.1175/JCLI-D-21-0059.1.

Zhang, T., Wang, T., Zhao, Y., Xu, C., Feng, Y., Liu, D., 2021b. Drivers of Eurasian Spring Snow-Cover Variability. J. Clim. 34, 2037–2052. https://doi.org/10.1175/JCLI-D-20-0413.1.

Zhang, S., Zeng, G., Yang, X., Iyakaremye, V., Hao, Z., 2022a. Connection between interannual variation of spring precipitation in Northeast China and preceding winter sea ice over the Barents Sea. Int. J. Climatol. 42 (3), 1922–1936. https://doi.org/10.1002/joc.7343.

Zhang, J.K., et al., 2022b. Impacts of stratospheric polar vortex changes on wintertime precipitation over the northern hemisphere. Clim. Dyn. 58, 3155–3171. https://doi.org/10.1007/s00382-021-06088-x.

Zhang, J., Wang, S., Huang, J., He, Y., Ren, Y., 2023a. The precipitation-recycling process enhanced extreme precipitation in Xinjiang, China. Geophys. Res. Lett. 50, e2023GL104324. https://doi.org/10.1029/2023GL104324.

Zhang, Y.J., Yin, Z.C., Wang, H.J., 2023b. Subseasonal transition of Barents-Kara Sea-ice anomalies in winter related to the reversed warm Arctic-cold Eurasia pattern. Atmos. Ocean. Sci. Lett. 16, 6. https://doi.org/10.1016/j.aosl.2023.100392.

Zhao, Y., Zhu, J., Xu, Y., 2014. Establishment and assessment of the grid precipitation datasets in China for recent 50 years (in Chinese). J. meteorol. Sci. 34, 414–420. https://doi.org/10.3969/2013jms.0008.

Zhao, J., Zhou, J., Yang, L., Hou, W., Feng, G., 2018. Inter-annual and inter-decadal variability of early- and late-summer precipitation over Northeast China and their background circulation. Int. J. Climatol. 38, 2880–2888. https://doi.org/10.1002/joc.5470.

Zhu, Y.L., 2011. A seasonal prediction model for the summer rainfall in Northeast China using the year-to-year increment approach. Atmos Oceanic Sci Lett 4, 146–150. https://doi.org/10.1080/16742834.2011.11446920.

Zhu, Z., Lu, R., Fu, S., et al., 2023. Alternation of the Atmospheric Teleconnections Associated with the Northeast China Spring Rainfall during a recent 60-year period. Adv. Atmos. Sci. 40, 168–176. https://doi.org/10.1007/s00376-022-2024-3.

Zuo, Z., Zhang, R., 2007. The spring soil moisture and the summer rainfall in eastern China. Chin. Sci. Bull. 52, 3310–3312. https://doi.org/10.1007/s11434-007-0442-3.

Zuo, Z., Zhang, R., 2016. Influence of soil moisture in eastern China on the East Asian summer monsoon. Adv. Atmos. Sci. 33, 151–163. https://doi.org/10.1007/s00376-015-5024-8.

Zuo, Z.Y., Yang, S., Wang, W.Q., Kumar, A., Xue, Y., Zhang, R.H., 2011. Relationship between anomalies of Eurasian snow and southern China rainfall in winter. Environ. Res. Lett. 6, 045402. https://doi.org/10.1088/1748-9326/6/4/045402.

Zuo, Z., Zhang, R., Wu, B., Rong, X., 2012. Decadal variability in springtime snow over Eurasia: Relation with circulation and possible influence on springtime rainfall over China. Int. J. Climatol. 32, 1336–1345. https://doi.org/10.1002/joc.2355.